HELSINGIN YLIOPISTO
HELSINGFORS UNIVERSITET
UNIVERSITY OF HELSINKI

Novel Therapeutic targets and biomarkers in Merkel Cell Carcinoma

Neurocan as a prognostic marker in Merkel Cell Carcinoma

University of Helsinki
Faculty of Medicine
Translational medicine
Programme
Master's thesis
April 2020
Marko Salmikangas
Supervisor: Harri Sihto

HELSINGIN YLIOPISTO
HELSINGFORS UNIVERSITET
UNIVERSITY OF HELSINKI

Tiedekunta – Fakultet – Faculty **Faculty of Medicine**		Koulutusohjelma – Utbildingsprogram – Degree Programme **International Master's program in Translational Medicine**
Tekijä – Författare – Author **Marko Salmikangas**		
Työn nimi – Arbetets titel – Title **Neurocan as a prognostic marker in Merkel Cell Carcinoma**		
Oppiaine/Opintosuunta – Läroämne/Studieinriktning – Subject/Study track **Cancer**		
Työn laji – Arbetets art – Level **Masters' thesis**	Aika – Datum – Month and year **April, 2020**	Sivumäärä – Sidoantal – Number of pages 73 (59 + 14)

Tiivistelmä – Referat – Abstract

Background

Merkel Cell Carcinoma (MCC) is a rare neuroendocrine tumor that is associated with old age and immunosuppressive condition. It has two distinct subgroups differentiated with their Merkel Cell Polyomavirus (MCPyV) positivity/negativity. While both groups are considered aggressive, the Merkel cell Polyomavirus negative group has significantly worse prognosis. Traditionally MCC cases have been diagnosed based on their physiological appearance and immunohistochemical markers such as cytokeratin 20 and tumor transcription factor-1, which differentiate MCCs from small cell carcinomas. It still requires skilled personnel such as dermatologists and pathologists to identify MCCs. More precise and effective biomarkers are required to improve MCC diagnostics, to enhance patient survival and in the development of personalized medicine for MCC.

Neurocan (NCAN) is a chondroitin sulphate proteoglycan that is found mainly in central nervous tissue in adults. The core protein of Neurocan is formed of 3 domains, G1 containing a single immunoglobulin domain, the glycosaminoglycan binding backbone and G3 domain containing regulatory protein-like sequences and epidermal growth factor/lectin-like domains. It is produced mainly by reactive astrocytes and its main function is to guide the growth of axons and to participate in the formation of neural extracellular matrix. Neurocan is linked to inhibition of axonal regeneration and glial scarring in case of neural injury. There are few mentions of Neurocan changes related to cancer outside of the central nervous system, however, there is clear evidence of chondroitin sulphate proteoglycan involvement in tumor invasiveness and potentially promotion of malignant tumor phenotype.

Aim of the study and experimental design

This thesis is a part of a project studying novel biomarkers and therapeutic targets for MCC. The aim of the study was to identify a novel cancer specific gene (Neurocan) that would be either a potential biomarker or therapeutic target, and to set up the pipeline for further expanding the parent project.

Neurocan was first identified from outlier gene detection methods applied to MCC sample series containing samples of 141 MCC patients. After this Neurocan expression levels were studied at protein level using immunohistochemistry for MCC sample series. NCAN expression levels in MCC cell lines were investigated at mRNA and protein level with qPCR and Western blotting respectively. Functional studies of Neurocan such as an effect on cell proliferation were performed with siRNA knockdown assays, and analyzed with Western blotting and qPCR.

Results

144 FFPE samples in TMA (tissue microarray) format were stained for Neurocan protein expression; 31 samples expressed NCAN at low level, 60 at intermediate level and 53 cases had high NCAN expression. The low NCAN expression correlated with poor MCC specific survival (5-year survival 44%) when compared to intermediate and high expression groups (5-year survival 73% and 65% respectively). Kaplan-Meier survival analysis also implicated a significant difference in survival between the groups, p-value 0.044. NCAN expression levels had a strong association with Merkel Cell Polyomavirus (MCPyV) status (Pearson Chi-square, p-value = 0.006) with 83% of high NCAN expression cases being MCPyV positive, where as 55% of low NCAN expression cases were MCPyV negative. Cox proportional hazards model revealed that NCAN is unlikely to be an independent variable in patient survival.

NCAN expression correlated with the MCPyV status of 9 tested MCC cell lines (Student's t-test, p-value = 0.041). Protein level studies were inconclusive due to lack of specific antibodies and testing methods.

4 cell lines were tested for NCAN functionality in cell cultures. siRNA knockdown of NCAN did not affect the survival of MCC cell lines, however, it had a reducing effect on Large T-antigen expression of the MCPyV positive cell lines. Likewise, siRNA knockdown of Large T-antigen reduced the expression of NCAN mRNA in MCPyV positive cell lines. No such interactions were found in the MCPyV negative cell lines. siRNA knockdown of sT-antigen significantly reduced the growth of MCPyV positive WaGa cell line (Student's t-test, p-value = 0.01). NCAN and large T-antigen targeting siRNAs had only a minor growth reducing effect on WaGa cell lines, and MKL1 cell line saw only minor growth reduction with all of the different siRNA treatments. These were not statistically significant findings. Whether Neurocan expression is directly controlled by MCPyV T-antigens, or whether the regulation is due to a signaling cascade of sorts, is still unknown.

Avainsanat – Nyckelord – Keywords
biomarker, cancer, Neurocan, Merkel cell carcinoma, Merkel cell polyomavirus

Ohjaaja tai ohjaajat – Handledare – Supervisor or supervisors
Harri Sihto, Adj. Prof. University of Helsinki, Faculty of Medicine

Säilytyspaikka – Förvaringställe – Where deposited
University of Helsinki/Helda E-Thesis

Muita tietoja – Övriga uppgifter – Additional information

Table of contents

Abbreviations

ABCG2 = ATP Binding Cassette Subfamily G Member 2 (Junior Blood Group)

AIDS = Acquired immune deficiency syndrome

Akt = AKT Serine/Threonine kinase 1

ATP = Adenosine triphosphate

BCAN = Brevican

cDNA = Complementary deoxyribonucleic acid

CD44 = CD44 molecule (Indian blood group)

CNS = Central nervous system

COPA = Cancer outlier profile analysis

CS = Chondroitin sulphate

CSPG = Chodroitin sulphate proteoglycan

DEG = Differentially expressed gene

DGIdb = Drug-Gene interaction database

DNA = Deoxyribonucleic acid

ECM = Extracellular matrix

EGFR = Epidermal growth factor receptro

eIF4E = Eukaryotic Translation Initiation Factor 4E

eIF4F = Eukaryotic Translation Initiation Factor 4F

E2F = E2F transcribtion factor

E4-BP1 = Eukaryotic Translation Initiation Factor 4E Binding Protein 1

FFPE = Formalin-fixed paraffin embedded

GAG = Glycoseaminoglycan

GAPDH = Glyceraldehyde 3-phosphate dehydrogenase

GFP = Green fluorescent protein

HGNC = HUGO Gene Nomenclature Committee

HIV = Human immunodeficiency virus

HRP = Horse radish peroxidase

IgG = Immunoglobulin gamma

IHC = Immunohistochemistry

Ki-67 = Cell proliferation marker Ki-67

KSPG = Keratin sulphate proteglycan

LAR = Leukocyte common-antigen related receptor family

LXCXE = LXCXE motif

LT = Large T-antigen

MCC = Merkel Cell Carcinoma

MCPyV = Merkel Cell Polyomavirus

MMP-2 = Matrix metalloprotease 2

mRNA = messenger RNA

mTOR = Mammalian target of rapamycin

NCAN = Neurocan

NG2 = Chondroitin Sulfate Proteoglycan 4

NSCLC = non-small cell lung cancer

NOTCH1 = Notch receptor 1

OCT4 = Octamer-binding transcription factor 4

OMIM = Online Mendelian Inheritance in Man

PAX 5 = Paired box gene 5

PI3K = Phosphoinositide 3-kinase

PRUNE2 = Prune Homolog 2

PTPRG = Protein Tyrosine Phosphatase Receptor Type G

PVDF = Polyvinylidene fluoride

p21 = Cyclin Dependent Kinase Inhibitor 1A

p53 = Tumor protein 53

p107 = RB Transcriptional Corepressor Like 1

p130 = RB Transcriptional Corepressor Like 2

qPCR = Quantitative polymerase chain reaction

RNA = Ribonucleic acid

RT = Radiation therapy

RT’ = Room temperature

SDS =Sodium dodecyl sulphate

PAGE = Polyacrylamide gel electrophoresis

shRNA = short hairpin RNA

siRNA = Small interfering RNA

sT = small T antigen

TdT = terminal deoxynucleotidyl transferase

TMA = Tissue microarray

VCAN = Versican

WB = Western blotting

Abstract

Background

Merkel Cell Carcinoma (MCC) is a rare neuroendocrine tumor that is associated with old age and immunosuppressive condition. It has two distinct subgroups differentiated with their Merkel Cell Polyomavirus (MCPyV) positivity/negativity. While both groups are considered aggressive, the Merkel cell Polyomavirus negative group has significantly worse prognosis. Traditionally MCC cases have been diagnosed based on their physiological appearance and immunohistochemical markers such as cytokeratin 20 and tumor transcription factor-1, which differentiate MCCs from small cell carcinomas. It still requires skilled personnel such as dermatologists and pathologists to identify MCCs. More precise and effective biomarkers are required to improve MCC diagnostics, to enhance patient survival and in the development of personalized medicine for MCC.

Neurocan (NCAN) is a chondroitin sulphate proteoglycan that is found mainly in central nervous tissue in adults. The core protein of Neurocan is formed of 3 domains, G1 containing a single immunoglobulin domain, the glycosaminoglycan binding backbone and G3 domain containing regulatory protein-like sequences and epidermal growth factor/lectin-like domains. It is produced mainly by reactive astrocytes and its main function is to guide the growth of axons and to participate in the formation of neural extracellular matrix. Neurocan is linked to inhibition of axonal regeneration and glial scarring in case of neural injury. There are few mentions of Neurocan changes related to cancer outside of the central nervous system, however, there is clear evidence of chondroitin sulphate proteoglycan involvement in tumor invasiveness and potentially promotion of malignant tumor phenotype.

Aim of the study and experimental design

This thesis is a part of a project studying novel biomarkers and therapeutic targets for MCC. The aim of the study was to identify a novel cancer specific gene (Neurocan) that would be either a potential biomarker or therapeutic target, and to set up the pipeline for further expanding the parent project.

Neurocan was first identified from outlier gene detection methods applied to MCC sample series containing samples of 141 MCC patients. After this Neurocan expression levels were studied at protein level using immunohistochemistry for MCC sample series. NCAN expression levels in MCC cell lines were investigated at mRNA and protein level with qPCR and Western blotting respectively. Functional studies of Neurocan such as an effect on cell proliferation were performed with siRNA knockdown assays, and analyzed with Western blotting and qPCR.

Results

144 FFPE samples in TMA (tissue microarray) format were stained for Neurocan protein expression; 31 samples expressed NCAN at low level, 60 at intermediate level and 53 cases had high NCAN expression. The low NCAN expression correlated with poor MCC specific survival (5-year survival 44%) when compared to

intermediate and high expression groups (5-year survival 73% and 65% respectively). Kaplan-Meier survival analysis also implicated a significant difference in survival between the groups, p-value 0.044. NCAN expression levels had a strong association with Merkel Cell Polyomavirus (MCPyV) status (Pearson Chi-square, p-value = 0.006) with 83% of high NCAN expression cases being MCPyV positive, where as 55% of low NCAN expression cases were MCPyV negative. Cox proportional hazards model revealed that NCAN is unlikely to be an independent variable in patient survival.

NCAN expression correlated with the MCPyV status of 9 tested MCC cell lines (Student's t-test, p-value = 0.041). Protein level studies were inconclusive due to lack of specific antibodies and testing methods.

4 cell lines were tested for NCAN functionality in cell cultures. siRNA knockdown of NCAN did not affect the survival of MCC cell lines, however, it had a reducing effect on Large T-antigen expression of the MCPyV positive cell lines. Likewise, siRNA knockdown of Large T-antigen reduced the expression of NCAN mRNA in MCPyV positive cell lines. No such interactions were found in the MCPyV negative cell lines. siRNA knockdown of sT-antigen significantly reduced the growth of MCPyV positive WaGa cell line (Student's t-test, p-value = 0.01). NCAN and large T-antigen targeting siRNAs had only a minor growth reducing effect on WaGa cell lines, and MKL1 cell line saw only minor growth reduction with all of the different siRNA treatments. These were not statistically significant findings. Whether Neurocan expression is directly controlled by MCPyV T-antigens, or whether the regulation is due to a signaling cascade of sorts, is still unknown.

Keywords: biomarker, cancer, Neurocan, Merkel cell carcinoma, Merkel cell polyomavirus

Review of the literature

Merkel Cell Carcinoma

C. Toker first used “trabecular carcinoma of the skin” in 1972 to describe a malignant skin cancer found in five elderly patients (Toker 1972). It showed neural crest origin and resembled Merkel cells when studied with electron microscopy six years later (Tang, Toker 1978). The original name was questioned and eventually the name Merkel cell carcinoma (MCC) prevailed. However, there is still controversy about the origin of MCC. In 2013 Axel zur Hausen et al. reported that majority of MCC cases express terminal deoxynucleotidyl transferase (TdT) and paired box gene 5 (PAX 5) which, when co-expressed, would indicate that the cell of origin for MCC has to be pro/pre- or pre-B cells (zur Hausen, Rennspiess et al. 2013). While this is true, there are multiple studies favoring the hypothesis that MCC has origin in stem cells. For example, there are multiple studies demonstrating that MCCs could differentiate from squamous or sarcomatous tissues (Hwang, Alanen et al. 2008, Walsh 2001) and others suggest neural crest origin (Grim, Halata 2000, Szeder, Grim et al. 2003).

Clinical features

MCC is often described as a rare neuroendocrine skin cancer that is associated with old age and immunosuppressive conditions. Other exposing factors include ultraviolet radiation and Merkel Cell Polyomavirus (MCPyV), the latter of which is a major contributor in tumorigenesis of MCC (Feng, Shuda et al. 2008, Sihto, Kukko et al. 2009, Becker, Schrama et al. 2008). A staggering 97% of MCC patients in Finland and in the United States are over 50 years old with more than 2/3 patients being over 70 years old at the time of diagnosis (Lemos, Storer et al. 2010, Kukko, Böhling et al. 2012). The age-adjusted incidence rate of MCC varies heavily, and is clearly associated with the availability of sunlight throughout the year. This is demonstrated by the annual incidence rates of Finland (1.2 per million) versus Australia (8.2 per million) and Detroit (0.22/100 000) versus Seattle (0.9/100 000). (Kukko, Böhling et al. 2012, Hodgson 2005, Girschik, Thorn et al. 2011)

In the National Cancer Data Base people with ethnical background were found to comprise of only 3,8% of all MCC patients, compared to the vast majority (96,2%) of people with Caucasian background (Lemos, Storer et al. 2010). In a Finnish study cohort men and women had similar MCC incidence rates (Kukko, Böhling et al. 2012), but in cohorts from United States and Australia, men had slightly higher incidence rate (61,3% and 65% males, respectively) (Girschik, Thorn et al. 2011, Lemos, Storer et al. 2010).

Most of the MCC lesions are non-tender (88%) and expand rapidly on a 3 month scale (63%)(Heath, Jaimes et al. 2008). While the majority of MCCs are considered a local disease at presentation, with only 14% of cases in Finland having a

metastasized cancer at presentation, the cancer is often fast to spread. In a Finnish study 38% of treated MCC cases with stage I or II cancer had a recurrence, out of which over a third (35%) had a recurrence with either a local or distant metastasis. The stage of the cancer has a drastic effect on patient survival, with patients staged I or II (at presentation) having a 5-year survival rate of over 67%, compared to stage III (metastasized disease) cancers 5-year survival rate of 17%. The study used American Joint Committee on Cancer TNM (tumor size/nodal status/metastasis) staging system from 2009, which has since been updated, however, the stages have remained similar in the most recent version from 2019. (Kukko, Böhling et al. 2012, American Cancer Society 2019)

Most of MCCs are located at the head and neck area or other UV exposed sites (70-90%). MCC patients have also been reported to have over 30-fold chance of having chronic lymphatic leukemia. (Heath, Jaimes et al. 2008) Other immunosuppression conditions such as HIV/AIDS have also been known to increase the risk of MCC. In 2002 Engels et al. reported that in a cohort of 309 365 patients from the United States, patients with AIDS had 13,4 times higher relative risk to develop MCC than general population. (Engels, Frisch et al. 2002) It is also known that therapeutic immunosuppression heightens the risk of MCC. Immunosuppressed MCC patients are also often younger than average MCC patients, with 49% of them being under 50 years old. (GOOPTU, WOOLLONS et al. 1997, Koljonen 2006)

Treatment and outcome

Surgical resection of the primary tumor is most often the first line therapy for MCC. A surgical margin of 2-3cm is suggested to achieve clear histologic margins, however, there is evidence that surgical margins of 1-2cm are enough and further expansion of the margins has no additional benefit to patient survival. Local recurrence is common and, even in patients with wide excision margins, the rate of local recurrence is between 25-40%. (Kukko, Böhling et al. 2012, Tello, Coggshall et al. 2018)

Second line in MCC therapy is radiation therapy (RT). Depending on the location of the tumor and the morbidity of surgery, radiation therapy can be used as a primary therapy option as well. A retrospective study by Bhatia et al. showed that hazard ratios for Stage I and II MCCs did not differ statistically between only surgery and primary radiation therapy. However, as an adjuvant therapy, RT reduced the risk significantly. Another study proved that local and nodal relapse rates of MCC were also similar between resection and radiotherapy (8.2% vs 11 % local and 33% vs 21 % nodal relapse, respectively). The NCCN (National Comprehensive Cancer Network) recommends radiation dosages between 50-66Gy, depending on the status of the patient and the usage of radiotherapy in MCC treatment (50 Gy as adjuvant therapy combined to surgery with negative margins vs 66 Gy for primary therapy at a non-resectable location). Table 1 is an excerpt from Bhatia et al. visualizing their findings. (Bhatia, Storer et al. 2016, Harrington, Kwan 2014, Tello, Coggshall et al. 2018)

	Stage I(n = 3369) (1341 deaths)		Stage II(n = 1474) (800 deaths)	
Treatment	**HR (95% CI)**	***P****	**HR (95% CI)**	***P****
Surgery/radiation				
Surgery only	1.0	–	1.0	–
Surgery + radiation	0.71 (0.64 to 0.80)	<.001	0.77 0.66 to 0.89)	<.001
Radiation only	0.92 (0.65 to 1.30)	.62	1.03 (0.73 to 1.46)	.85

Table 1. Hazard ratios of different treatments for MCC. HR = hazard ratio, CI = confidence interval. (Bhatia, Storer et al. 2016)

Other adjuvant therapies for MCC include chemotherapy, which is used mainly in palliative treatment. While initial responses to traditional chemotherapy (i.e. cisplatin and doxorubicin) are decent (53-76%), the effect is often short lived and cancer progression occurs within 3-8 months (Voog, Biron et al. 1999). Chemotherapies are also often poorly tolerated and cause adverse side effects such as skin toxicities for 63% of patients (Garneski, Nghiem 2007). And while modern immune therapies have proven effective in the treatment of some Merkel Cell Carcinomas, roughly 50% of Merkel Cell Carcinomas are resistant to these therapies (Pembrolizumab: overall response rate 50%; Avelumab: overall response rate 33%). Furthermore, half of the patients who get initial response to immune therapies relapse and become resistant to the treatments eventually. (Miller, Church et al. 2018, Femia, Prinzi et al. 2018, Harms, Paul W., Harms et al. 2018)

Merkel Cell Polyomavirus

Merkel Cell Polyomavirus (MCPyV) is the fifth recognized human polyomavirus, out of the 13 human polyomaviruses known today (Calvignac-Spencer, Feltkamp et al. 2016, Feng, Shuda et al. 2008). It belongs to the *polyomaviridae* family of viruses, a group of non-enveloped viruses with icosahedral capsids. They are fairly small, only 40-45nm in diameter, and contain a circular double stranded DNA molecule of roughly 5kbp. Like other polyomaviruses, MCPyV genome contains a unique origin of replication (ORI) from where transcription can start bidirectionally. On one side the transcription of so called early genes leads to non-capsid proteins, often referred as the T-antigens, more of which will be discussed later. Capsid proteins VP1,VP2 and VP3 are transcribed from the other direction. Although the core structure of MCPyV is similar to other human polyomaviruses, Feng et al. reported that the closest relative to MCPyV based on their initial cDNA sequencing was the African green monkey virus. Figure 1 visualizes the structure of MCPyV genome as described by Feng et al. (Feng, Shuda et al. 2008, Johne, Buck et al. 2011)

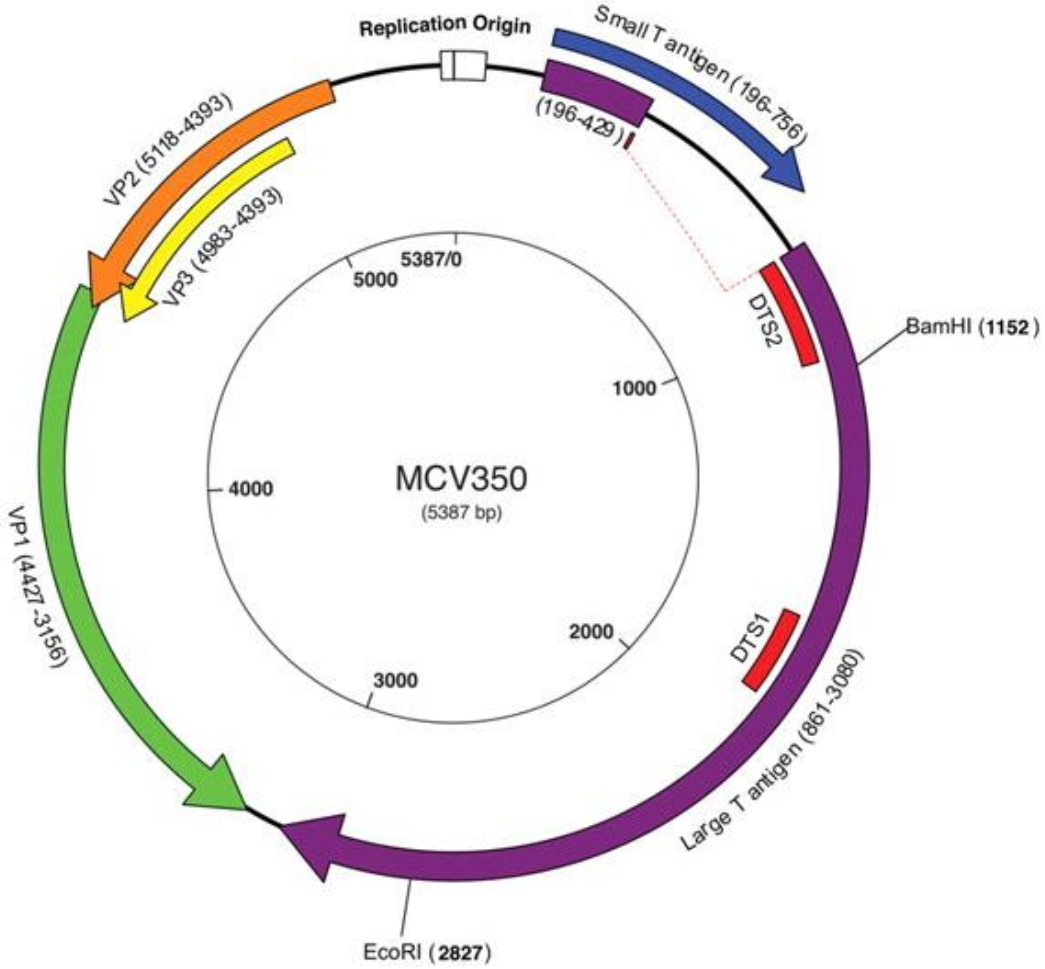

Figure 1. Merkel Cell Polyomavirus (Feng, Shuda et al. 2008).

The name Merkel Cell Polyomavirus stems from the fact that MCPyV was originally discovered by Feng et al. from cDNA sequences of MCC patient samples. They hypothesized that as MCC resembles Kaposi's sarcoma, as both are overexpressed in immunocompromised patients, it might have similar mechanisms of tumorigenesis behind it. And as Kaposi's sarcoma has been found to associate with a herpesvirus infection (Chang, Cesarman et al. 1994), they decided to check whether MCC samples would contain any viral cDNA. Out of 10 MCC patient samples 8 proved to be positive for a yet unknown virus, where as only 8,5% of control tissues from various sites and 16% of normal skin samples from immunocompromised patients and non-MCC skin tumors contained detectable amounts of this virus. (Feng, Shuda et al. 2008)

The T-antigens in MCPyV can be spliced into three different variants: the large T-antigen, the small T-antigen and 57kT antigen. These T-antigens are known to have oncogenic properties, as they target tumor suppressor proteins such as the retinoblastoma protein (Rb), p53 and protein phosphatase 2 a (PP2A). While T-antigens are evident in all MCPyV positive MCCs, there are unique variations to them, especially in the case of LT. In a study by Shuda et al. 2008, 9 out of 9 MCCs harbored unique LT truncating mutations, where as in control samples of non-MCC origin 0 out of 4 samples had a LT truncating mutation. This is thought to play a role in tumor survival, as expression of viral antigens might lead to cell

cycle arrest, or tumor compromising immune response. (Feng, Shuda et al. 2008, Sihto, Kukko et al. 2009, Johne, Buck et al. 2011, Shuda, Feng et al. 2008)

MCC tumorigenesis

Soon after its discovery in 2008, MCPyV proved to be a key player in MCC tumorigenesis. Approximately 70-80% of MCCs are considered to be derived from MCPyV and the rest are mostly UV-radiation induced MCCs. Harms et al. discovered that in MCPyV negative MCCs, 85% of mutations are C>T transitions, a typical finding for UV-induced DNA damage (Harms, Paul William, Vats et al. 2015). They also showed that MCPyV negative tumors have a higher mutational burden and multiple mutations in known tumor suppressor genes such as p53, RB, NOTCH1 and PRUNE2. This has been shown to render proteins like p53 and RB non-functional in MCPyV negative MCCs, resulting in similar pathogenic mechanisms as in MCPyV positive MCCs (Sihto, Kukko et al. 2011). UV-radiation is also known to increase the small T-antigen levels in non-pathogenic MCPyV positive skin samples (Mogha, Fautrel et al. 2010). When combining these factors to the preferential localization of MCC to UV exposed sites, it is clear that UV-radiation is one of the most crucial factors in MCC tumorigenesis. (Harms, Paul William, Vats et al. 2015, Mogha, Fautrel et al. 2010, Koljonen 2006)

Other important factors in MCC tumorigenesis are the T-antigens in MCPyV positive MCCs. The large T-antigen and small T-antigen are studied frequently where as the 57kT-antigens functions are fairly unknown. The 57kT-antigen is known to contain a DnaJ binding domain, which in highly similar 17kT-antigen of simian virus 40 (SV40) promotes cell cycle progression and cell proliferation (Boyapati, Wilson et al. 2003). Both also contain a RB binding domain (LXCXE domain) which can inhibit p130 and p107 proteins and activate E2F-transcription factor, promoting tumor growth (Boyapati, Wilson et al. 2003, Stubdal, Zalvide et al. 1997).

sT-antigens are highly conserved among polyomaviruses, and are often described to be involved in viral cell cycle and cell transformation (Khalili, Sariyer et al. 2008). While MCPyV sT-antigen has multiple functions in viral replication, two interactions stand out when tumorigenesis is considered. Firstly, MCPyV sT-antigen is known to target the translation regulator protein 4E-BP1, a downstream component of the PI3K-Akt-mTOR pathway (Shuda, Kwun et al. 2011). 4E-BP1 is primarily responsible for regulation of eIF4F translation initiating complex through its mRNA cap binding component eIF4E. This eIF4F complex has been shown to suppress tumorigenic activity when functioning normally, and the loss of the 4E-BP1 has been shown to lead to malignant cell growth. (Avdulov, Li et al. 2004)

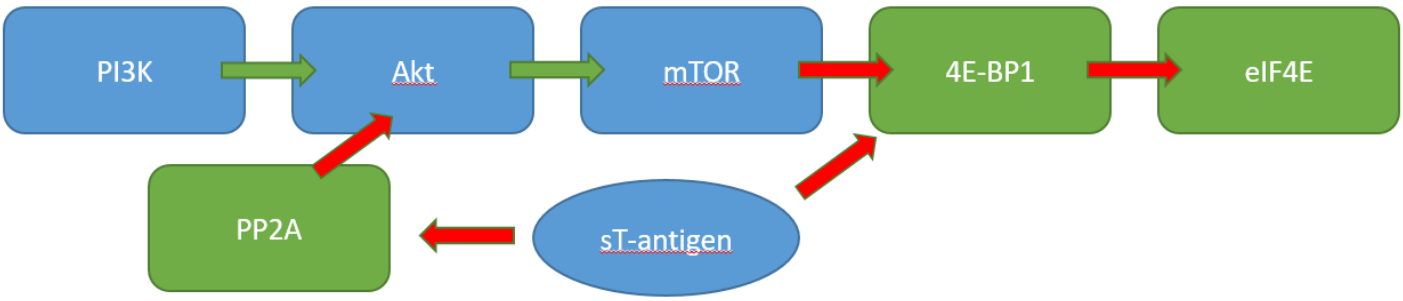

Figure 2. sT inhibition of PI3K-Akt-mTOR pathway. Red arrows indicate inhibitory interaction and green arrows indicate promotive interaction.

In addition to sT-antigens' ability to directly bind to 4E-BP1 it can also affect the upstream elements of the same pathway. MCPyV sT-antigen contains two PP2A binding domains, leading to activation of Akt through PP2A inactivation. As a well-known oncogenic pathway, the PI3K-Akt-mTOR has been well studied and shown to be a critical factor in viral carcinogenesis (Shuda, Kwun et al. 2011, Feng, Kwun et al. 2011, Shuda, Feng et al. 2008).

Lastly, the LT-antigen of MCPyV is the key players behind MCPyV tumorigenesis. While both 57kT and sT-antigens can affect crucial cellular functions independently as described previously, they are often merely supporting elements for the LT-antigen. The LT-antigen contains a DnaJ binding domain, two tumor suppressor protein domains (p53 and RB), origin binding domain and ATPase and helicase domains, as well as zinc finger and leucine zipper motifs. (Shuda, Feng et al. 2008) However, the LT-antigen is often truncated, leading to inability of viral reproduction as a result of losing the origin binding and/or ATPase/helicase domains, as well as reduced functionality due to loss of, for example, p53 binding domain (Borchert, Czech-Sioli et al. 2014).

In MCC tumorigenesis, two LT-antigen domains stand out from the rest, the p53 and RB binding domains. While p53 domain of MCPyV LT-antigen is often incomplete or completely truncated, studies have shown that MCPyV LT-antigen can indirectly reduce p53 activity in cell lines (Borchert, Czech-Sioli et al. 2014). This can result in uncontrolled growth and lack of apoptosis in cells (Sullivan, Pipas 2002). As Figure 3 visualizes, p53 restricts cell cycle by causing G2 and G1 growth arrest through signaling cascade involving p21, and can cause bax-mediated apoptosis, if a cell undergoes excess DNA damage (Sullivan, Pipas 2002).

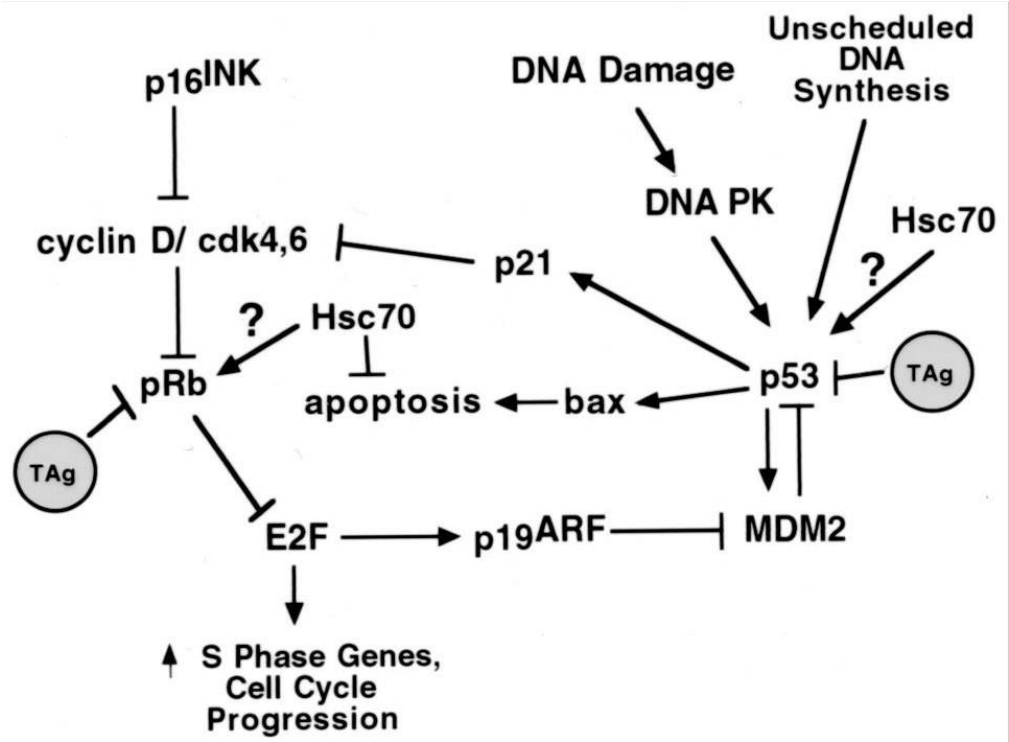

Figure 3. Inhibition of tumor suppressor pathways by T-antigens by Sullivan et al. (Sullivan, Pipas 2002)

Another tumor suppressor protein, RB, often has a complete binding domain despite of the LT-antigen truncations. Interestingly, truncated LT-antigens showed even greater affinity to RB compared to a full length LT-variant (Borchert, Czech-Sioli et al. 2014). Many cancers exploit the RB-E2F interaction by either mutating the RB protein or by affecting the up-/downstream signaling of the RB. This causes E2F mediated transcription, leading to production of S-phase genes and eventual cell cycle progression. (Sherr 2000)

Neurocan

Neurocan (NCAN) or *CSPG3* is a nervous tissue specific proteoglycan thought to be important in cell-to-cell and cell-to-matrix interactions. It consists of a core protein and one or more glycosaminoglycan (GAG) sidechains. The gene coding for the Neurocan protein is located in chromosome 19 and spans over nearly 1Mb of 19p12-13.1. It consists of 15 exons forming an open reading frame that consist of 3963 base pairs or 1321 amino acids. The exons 3-6 are used to code for the N-terminal of Neurocan and exons 9-14 are used to code for the C-terminal. These regions show high homology with other members of the proteoglycan family (50% and 72% respectively) as well as with different species (92% both). Exons 7 and 8 are used for the central portion and have no significant homologies with other proteoglycans nor species, with the exception of mouse and rat Neurocan protein having 57% (exon 7) and 29% (exon 8) homology.

The N-terminus (G1 domain) of Neurocan is comprised of a single immunoglobulin domain followed by multiple tandem repeats, whereas the C-terminus (G3 domain) is comprised of one or two epidermal growth factor-like domains, a lectin-like domain, and a regulatory protein-like sequence. Between these lies the CS-

GAG backbone, onto which one or more chondroitin sulphate glycosaminoglycan (CS-GAG) polysaccharides attach. While the primary structure is similar in proteoglycans, the central portions are unique to each proteoglycan. The size of proteoglycan core proteins varies between 95 kDa to 400 kDa and the number of CS-GAGs can be anything between 1 and 100 units. (Prange, Pennacchio et al. 1998, Lau, Cua et al. 2013) Figure 4 by Lau et al. visualizes the general structure of lecticans including Neurocan.

Rauch et al (1995) reported that Neurocan protein concentrations are highest in neonatal rat brains comprising 20% of all chondroitin sulphate proteoglycans while in adult rats the amount is 6%. (Rauch, Grimpe et al. 1995) The protein is developmentally regulated in other fashions as well. For example, the molecular weight of rat fetus Neurocan protein is 245kDa, where as in 7-day-old rats the predominant form has a molecular weight of 150kDa. (Prange, Pennacchio et al. 1998) This indicates the importance of the protein during fetal/embryonal development.

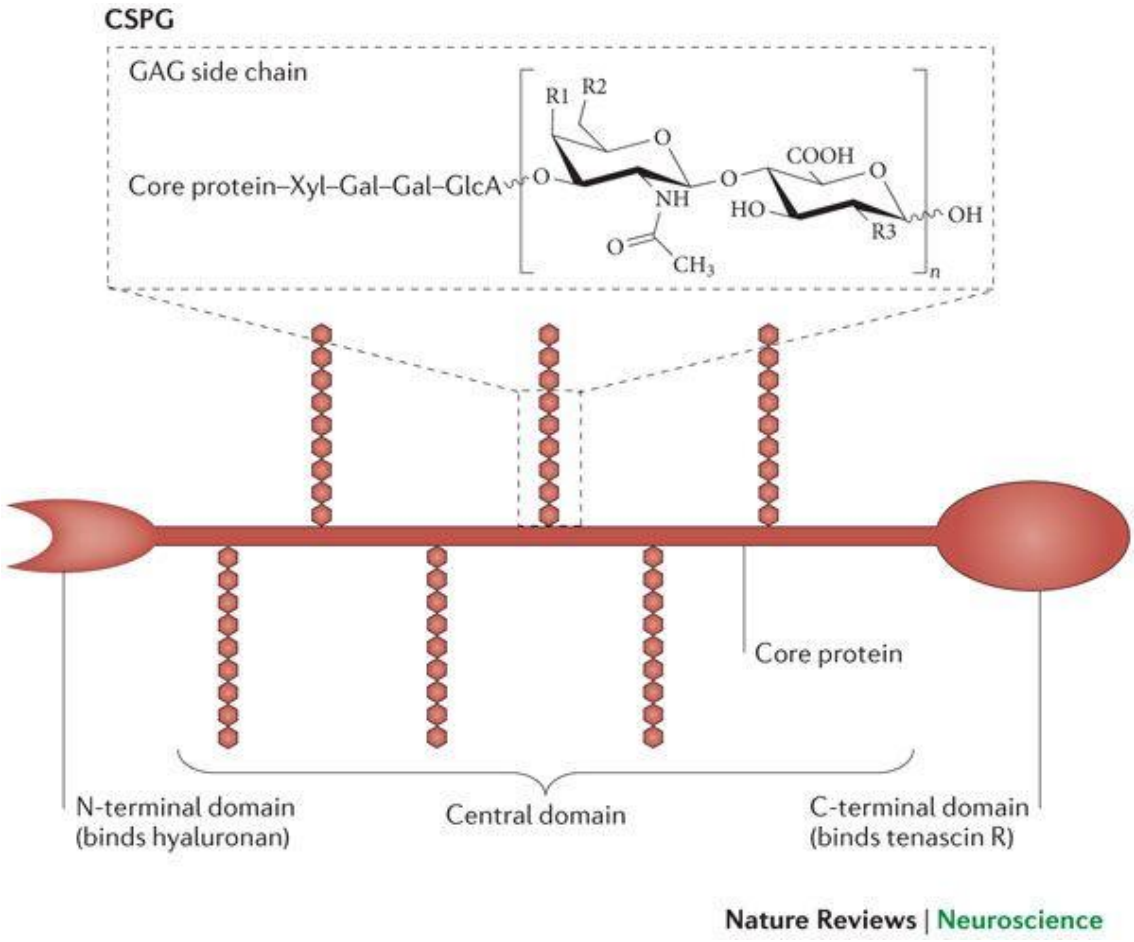

Figure 4. CSPG structure by Lau et al. (Lau, Cua et al. 2013)

Functions of Neurocan protein

The main function of NCAN protein is to guide axonal growth and to stabilize the extracellular matrix of central nervous system. While we are focused on Neurocan, other CSPGs as well as hyaluronan and tenascin-R are essential for both

of these functions described hereafter. For the axonal growth guidance, two methods of action have been proposed by which this could happen. Method 1 is based on axon inhibition, where as method 2 relies on “addictive” growth of axons in CSPG rich areas. In method 1, CSPGs form a dense barrier around target areas and force the growing axons to divert from their path. (Silver, D. J., Silver 2014) This sort of behavior has been shown to happen during development, for example, when CSPG barriers block axons from protruding through spinal cords roof plate (Snow, Steindler et al. 1990)

This is also a form of protection during CNS injury. Reactive astrocytes have been shown to form a barrier around injured area or CNS lesions. This barrier consists not only from the reactive astrocytes themselves, but also of intermediate filament proteins and astrocyte produced CSPGs and KSPGs (keratin sulphate proteoglycans). The main purpose of these barriers is to isolate the injured area from healthy tissue to prevent the damage from spreading while also protecting the damaged area from excess inflammation causing unrecoverable cell damage. (Silver, J., Miller 2004)

The second method involves CSPG preferential receptors on, for example, migrating neuroblasts and extending axons. Neurons grown together with Schwann cells expressing CSPGs tend to grow axons along the Schwann cells, but when the CSPG expression is diminished or the CS-GAG chains of the CSPGs are degraded, the growth patterns change. The axons can completely abandon the Schwann cells, and can start infiltrating surrounding cells/tissues (Silver, D. J., Silver 2014, Grimpe, Pressman et al. 2005, Kuffler, Sosa et al. 2009). Interestingly, even though the axons seem to prefer the Schwann cells when expressing CSPGs, the growth of the axons can multiply by up to 11-fold when treated with Chondroitinase-ABC, which cleaves the N-acetyl glucosamine and glucouronic acid units apart from the CS-GAG backbone (Grimpe, Pressman et al. 2005).

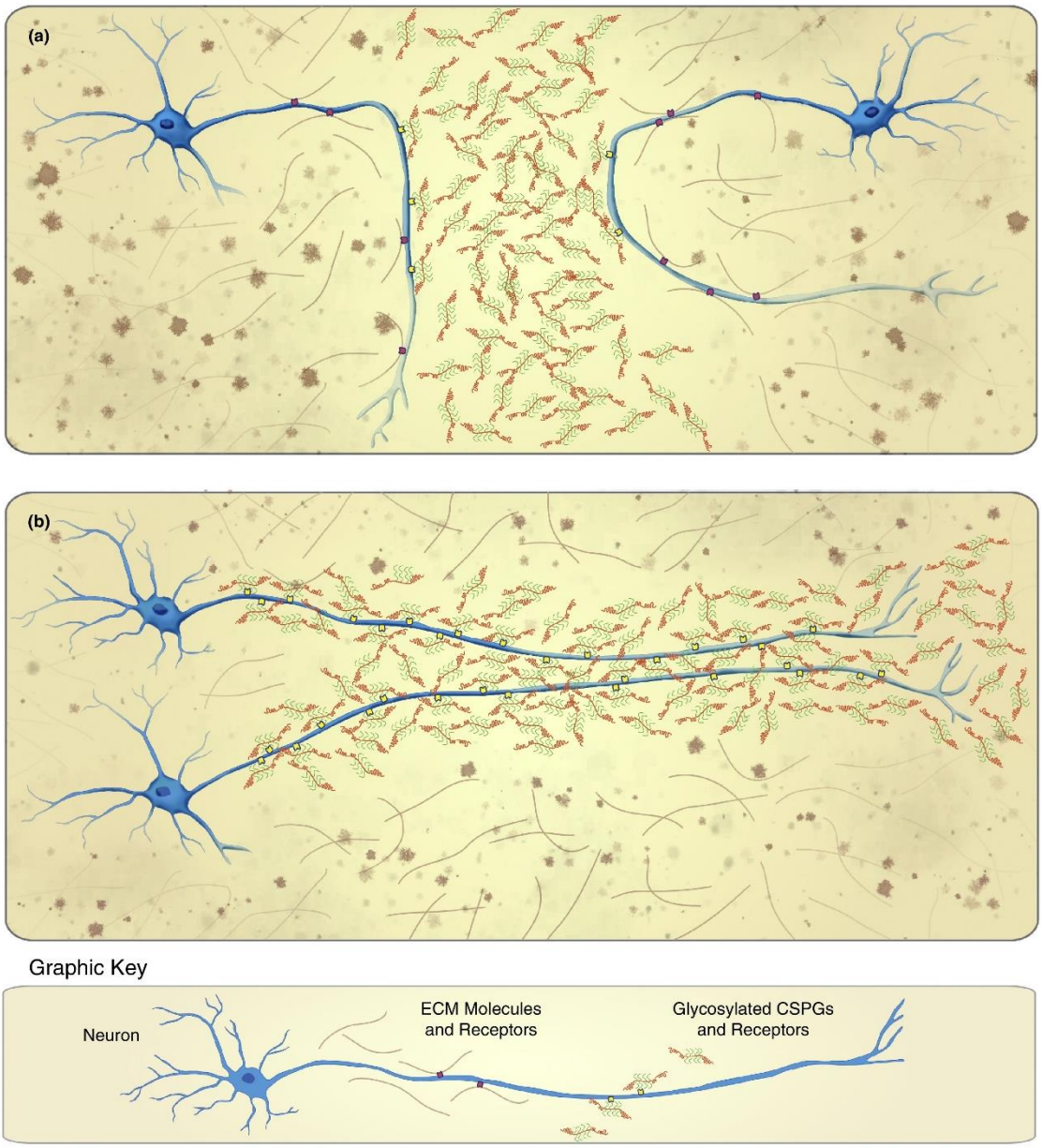

Figure 5. Axonal guidance by CSPGs by Silver et al. a) represents the inhibitory turning pattern of CSPG mediated axonal growth (method 1) where as b) represents the "addictive" growth pattern, method 2. (Silver, D. J., Silver 2014)

This can also backfire, as is case in glial scarring. Axonal regrowth is hindered by entrapment of axons by neural glia expressing NG2 (CS-GAG receptor), and this can cause permanent stall in the axonal growth. Studies have shown that these "traps" can be disarmed by cleaving the CS-GAGs from CSPGs with Chondroitinase-ABC, resulting in renewed axonal growth. However, this can be troublesome, since the presumed purpose of this sort of behavior and glial scarring, is to repair the severed blood-brain barrier and to limit the inflammatory responses in the area (Silver, J., Miller 2004). There is also evidence that cleavage of the CSPGs are behind invasive type brain tumors such as invasive glioma and invasive low-grade astrocytoma (Zhang, Kelly et al. 1998, Varga, Imre, Hutóczki et al. 2012). This will be discussed in more detail in the following chapter.

The other important function of Neurocan is to form perineural nets found in the ECM. CSPGs form one of the three major components of CNS ECM by attaching to hyaluronan and tenascin-R with their G1 and G3 domains respectively. (Silver, D. J., Silver 2014). These structures can further attach to laminin, fibronectin, collagen and even cell bodies of neurons and glial cells, forming a dense net in the CNS. During embryonal development proliferation, migration and forming of synapses (synaptogenesis) are possible due to the loose ECM structure in the CNS. This all changes in postnatal development, as ECM molecules such as CSPGs start forming perineural nets, surrounding synapses and bringing ECM molecules tighter together. This limits the plasticity of the CNS, enabling proper synaptic function for example. (McRae, Porter 2012, Lau, Cua et al. 2013, Silver, D. J., Silver 2014) Figure 6 visualizes these perineural nets as depicted by Lau et al. 2013.

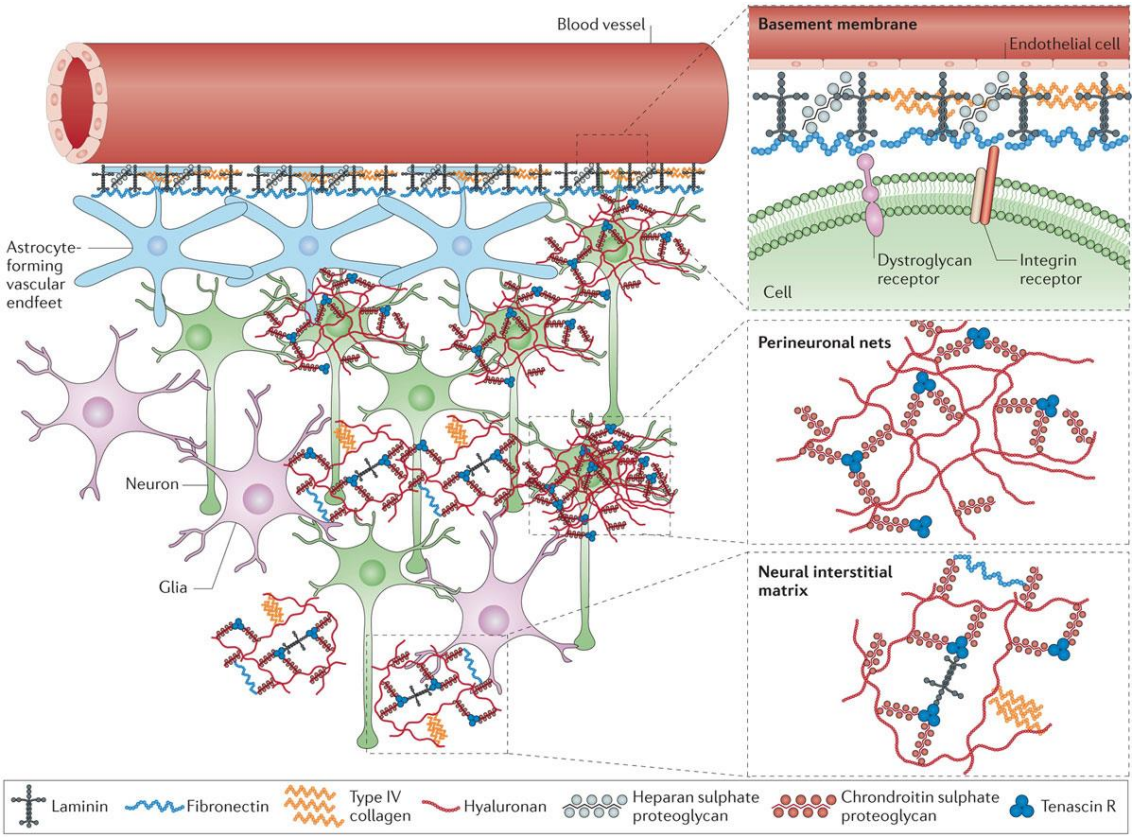

Figure 6. Extracellular matrix molecules and the perineural nets of CNS by Lau e al. (Lau, Cua et al. 2013)

Neurocan and cancer

While there are only a few studies directed towards NCAN in cancer, proteins from the same CSPG family (Brevican and Versican) have been studied and can shed light into NCANs potential tumorigenic properties. Studies of NCAN in cancer are mostly related to cancers with neural crest origin, and only one study to our knowledge has highlighted the potential association of NCAN with cancer as a single nucleotide polymorphism in NCAN gene associated with higher risk of hepatocellular carcinoma in a study by Nischalke et al. The NCAN rs2228603 polymorphism proved to be significantly more frequent in alcoholic liver disease related hepatocellular carcinoma (15.1%) compared to healthy controls (7.9%),

alcoholic and alcoholic cirrhosis controls (7.2% and 9.3% respectively) and hepatitis C virus associated hepatocellular carcinoma (9.1%). (Nischalke, Lutz et al. 2014) Whether this was a driving factor in the oncogenesis, or a collateral damage remained uncertain.

It is commonly known that tumors manipulate the surrounding cells and ECM to promote their growth and invasiveness (Henke, Nandigama et al. 2020). As NCAN is known to be responsible for the integrity of the ECM of CNS, as described previously, it is no surprise that its potential in tumor infiltration has been studied frequently. For example, Varga et al. reported that Neurocan alongside with Brevican, Versican and Tenascin-C would be responsible for invasive phenotype in low-grade astrocytoma. They compared the mRNA expression levels of normal brains, astrocytoma, schwannoma and intracerebral non-small cell lung cancer (NSCLC), and found that the before mentioned four proteins separated the infiltrative semi-malignant astrocytoma from the benign schwannoma and poorly infiltrating NSCLC metastasis. (Varga, Imre, Hutóczki et al. 2012)

In their earlier study, Varga et al. studied the invasion related ECM molecules in glioblastoma, and found that Tenascin-C, CD44 and MMP-2 were heavily involved in the infiltration potential of glioblastoma. While NCAN was not found to be significantly different between glioblastoma and normal brain, it is noteworthy, that Tenascin-C, CD44 and NCAN are all related via perineural net formation, where as MMP-2 is known to degrade both NCAN and CD44. (Varga, I., Hutóczki et al. 2010, Yao, Tucker et al. 2011, Frischknecht, Seidenbecher 2008) As shown previously, perineural nets are crucial in the stability of the ECM of CNS, which when tampered with can be potentially beneficial for tumor infiltration.

Another study illustrating the potential role of NCAN in metastasis focused on Brevican, a close relative of NCAN that shares many functions and is similar in structure to NCAN. (Silver, D. J., Silver 2014). Zhang et al. discovered that a cleaved Brevican protein induced tumor infiltration both *in vitro* and *in vivo.* Neonatal rat brains were implanted with otherwise non-invasive, non-Brevican expressing 9L glioma cell line, and transfected with either GFP (control), full length Brevican or a cleaved version of Brevican (Figure 7). In cell culture, cells treated with either full length or cleaved Brevican both showed increased invasiveness, but in rat xenografts, only cleaved Brevican showed increased cell infiltration. (Zhang, Kelly et al. 1998)

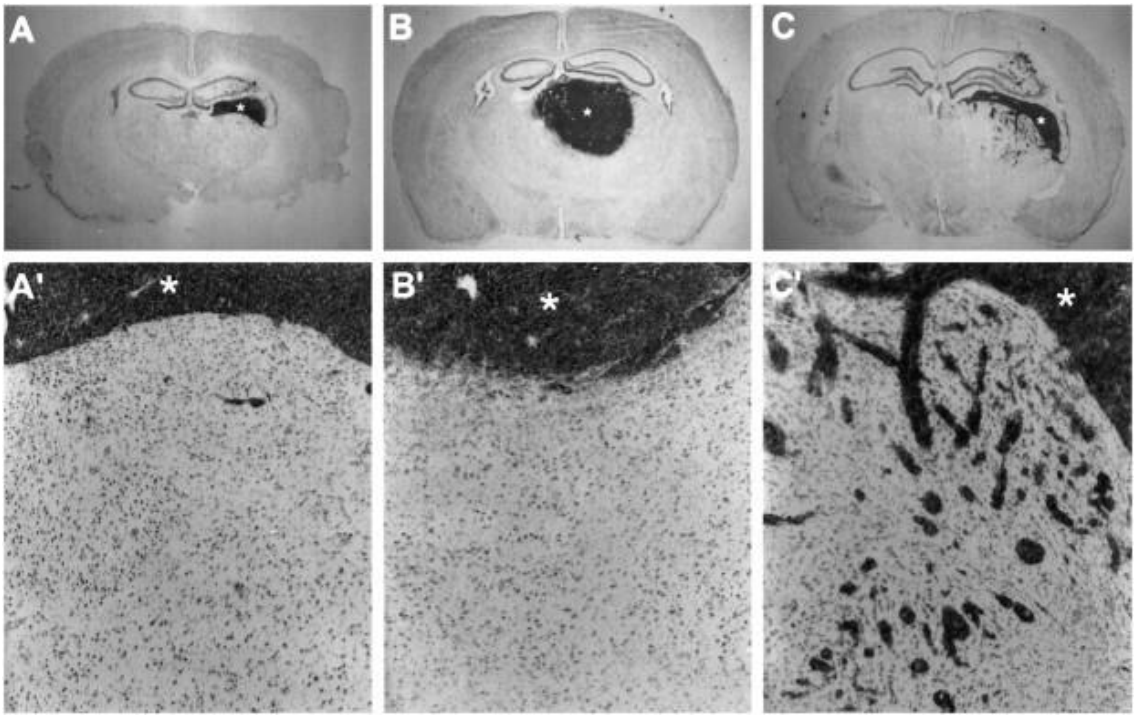

Figure 7. CSPG and tumor infiltration by Zhang et al. A (A') and B (B') tumors show little to no invasive cell clusters, where as C (C') tumor shows a lot of infiltrated cell clusters. A) 9L glioma cell line, intracranial injection. B) 9L cell line transfected with full form (functional) BEHAB/Brevican. C) 9L cell line transfected with HABD, a cleaved N-terminal version of Brevican. (Zhang, Kelly et al. 1998)

Stromal Versican (a member of the lecticans like Brevican and Neurocan) has been shown to associate with cancer inhibition through cancer-associated fibroblasts. Depletion of VCAN in mice xenografts showed decreased number of cancer-associated fibroblasts, resulting in thinner stromal barriers and unclear boundary around tumors. (Fanhchaksai, Okada et al. 2016) As described previously, one of the major functions of Neurocan and other CSPGs is isolation of injured areas by formation of barrier-like structures. As cancers often resemble lesions and other injuries (depending on its location), it is not surprising that the first reaction to this lesion like injury would be to treat them as lesions. So, barrier formation such as this could be one of the explaining factors to how CSPGs are linked to cancer invasiveness. Indeed, Silver et al. demonstrated that tumor infiltration of high-grade gliomas occurs in areas where CS-GAG-rich matrix is reduced (Silver, D. J., Siebzehnrubl et al. 2013). And as Zhang et al. highlighted, a complete Brevican protein is required for efficient inhibition of tumor invasiveness.

In a recent study, Su et al. discovered that high expression of NCAN is associated with poor prognosis in neuroblastoma. They also proved that exogenous NCAN could potentiate spheroidal growth of neuroblastoma cells, which is often associated with undifferentiated and malignant phenotype. The knockdown of NCAN resulted in growth reduction *in vitro*, and the mRNA levels of stem cell markers such as OCT4, Nestin and ABCG2 were reduced. (Su, Kishida et al. 2017) While these results may seem contradictory to the ones mentioned previously, it needs to be noted that CSPGs are known to be ligands for leukocyte common-antigen

related (LAR) receptor family, Protein Tyrosine Phosphatase Receptor (PTPR) family, and Epidermal Growth Factor Receptor (EGFR) for instance (Shen, Tenney et al. 2009, Lau, Cua et al. 2013). Some of these receptors are known to have cell transforming and oncogenic potential, so if CSPGs are overexpressed in wrong circumstances, the outcomes might be unforeseen. (Morris, Taylor et al. 2011)

Aims of the study

Identification of novel biomarkers and therapeutic targets for MCC

Rare Cancers Research group has acquired a vast amount of MCC patient samples and data (gene expression levels, outlier genes etc.) relating to these samples. This project is the first step of a larger study aiming to discover potential biomarkers and therapeutic targets in Merkel Cell Carcinoma. In the beginning of this project, the patient sample data was scrutinized, and one gene of interest (Neurocan) was identified to serve as a model for the upcoming studies.

Frequence and prognostic role of Neurocan expression in MCC

Protein expression levels of Neurocan was investigated in the MCC sample series with immunohistochemistry. Primarily, we investigated whether Neurocan protein expression relates to the findings in RNA sequencing, and if MCPyV positive tumors clearly differ from MCPyV negative tumors. This will verify the functionality of the bioinformatics pipeline, and support in the construction of a working biomarker identification pipeline for the parent project. Secondly, association between Neurocan protein expression and clinical features, such as cancer stage and patient survival was investigated, as this will be an indication of Neurocans' potential as a biomarker in MCC diagnostics.

Importance of neurocan in MCC tumorigenesis

After verifying the bioinformatics findings in the MCC patient sample series, we investigate the Neurocan expression in our MCC cell lines. The expression levels were analyzed primarily with qPCR and secondarily with Western Blotting. Furthermore, the role of Neurocan in MCC tumorigenesis was studied with methods of modern molecular biology. The studies included methods such as cell proliferation assays (cancer growth) and whether shutting down Neurocan with siRNA will affect cell viability and/or viral T-antigen expression.

Materials and Methods

MCC sample series

The MCC sample series is a collection of Merkel Cell Carcinoma patient samples from the Finnish cancer registry. This collection is the biggest population based MCC series, and holds over 200 patient samples collected between years 1983-2018. The collection has been gathered and is maintained in collaboration with Rare Cancers Research group and the Finnish Biobanks. Clinical features used in the project (such as patient survival, cancer stage and cancer location) were collected from the Finnish Cancer Registry.

MCC cell lines

10 Merkel Cell Carcinoma cell lines were used in this study, some of which were acquired from the European Collection of Authenticated Cell Cultures (ECACC), and others kindly provided by Dr. Roland Houben and Prof. Annamari Ranki. Out of these 10 cell lines 6 were Merkel Cell Polyomavirus positive: BroLi, MKL1, MKL2, MS1, PeTa and WaGa. The rest were Merkel Cell Polyomavirus negative: MCC13, MCC14/2, MCC26 and UISO. We also partly included a fifth polyomavirus negative cell line, ME212, which has been established recently in collaboration with Prof. Leif Andersson.

3' RNA sequencing

RNA for the sequencing was extracted from formalin-fixed paraffin embedded tissue (FFPE) blocks with QiaSymphony according to manufacturer's protocols. Prior to extraction, two 10 µm sections were dissected from the paraffin blocks and paraffin from the sections was removed. This was achieved by incubating the sections in +56°C in Qiagen deparaffinization solution (Qiagen #939018). After deparaffinization, proteinase K (Qiagen #19133) was added to inactivate endogenous RNAses and to start the cell lysing. This was followed with an hour-long incubation in +56°C on a shaker, and the following liquefied samples were then transferred into the QiaSymphony for processing. The RNA was then extracted with Qiagens ready-made protocol, "RNA_FFPE_130_V7 protocol", which comes pre-installed in the QiaSymphony.

The 3' sequencing was performed in collaboration with FIMM. RNA libraries for sequencing were prepared with QuantSeq 3' mRNA-Seq Library kit (Lexogen, Vienna, Cat.no.: 015.96) and sequenced using the NovaSeq 6000 instrument with with NovaSeq S1 XP NS1-200 protocol (Illumina Inc.) at the Institute of Molecular Medicine Finland (FIMM, Helsinki, Finland). Lexogen QuantSeq 3' workflow is introduced in Figure 8. MediSapiens ltd. analyzed the sequencing data. The QuantSeq sequencing technology is described elsewhere (Corley, Troy et al. 2019).

Figure 8. Lexogen QuantSeq 3' sequencing workflow (LexoGen 2019).

Data analysis of MCC RNA sequencing data

The data analysis (bioinformatics) of the sequencing data was performed in collaboration with MediSapiens ltd. The bioinformatics pipeline included SIBER analysis, Gene tissue indexing, Gene set enrichment analysis and IST ranking. These methods are described in other publications (Tong, Chen et al. 2013, Subramanian, Tamayo et al. 2005, Mpindi, Sara et al. 2011), except for IST ranking, which is developed by MediSapiens ltd. and has yet to be made publicly available. The IST ranking working principle, shortly, is as follows: gene expression of differently expressed genes is analyzed with deseg2 and the differently expressed genes (DEGs) are ranked by their expression. The following DEGs are filtered with 1,5 fold expression cut-off per subtype. The following gene list is then compared with lists from the IST-online database (normal and cancerous), and if a gene was represented in the top 500 highest expressed genes of either list, it was removed. The remaining list should be comprised of highly expressed and subtype specific genes. (MediSapiens ltd. 2019)

Immunohistochemistry

Tissue microarray samples (TMA) were prepared from patient samples and stained for Neurocan protein expression. The samples were first deprived of paraffin with descending alcohol series followed by endogenous peroxidase blocking with H_2O_2. The samples were then washed twice with TBS (5 minutes in room temperature [RT']) and heat-induced epitope retrieval (15 minutes in 95°C) was performed in EnVision™ Flex Target Retrieval solution Low pH buffer (Dako, REF K8005) with Biocare Medical Decloaking chamber. Two washes with TBS (5 min each) were administered and primary NCAN antibody (Atlas antibodies, HPA036814) was applied on the samples, diluted 1:1000 in Draco antibody diluent (WellMed, Cat.no.: AD500), and left to incubate overnight at +4°C. After two washes (TBS, 5 min each) horseradish peroxidase (HRP) conjugated secondary anti-Rabbit antibody (1 step detection system rabbit HRP [WellMed, Cat.no.: R500HRP]) was applied on the samples for one hour RT' followed by another two washes (TBS, 5 min each). Finally, the samples were stained with ImmPACT DAB Substrate kit (Vector laboratories, REF SK4105) and counterstained with hematoxylin. The complete immunohistochemistry protocol used in this study can be found in Appendix 2.

The stained TMAs were then digitalized in collaboration with Helsinki Biobank. The digitalized TMAs were analyzed for the intensity of their NCAN staining, correlating with the protein expression levels of NCAN. The samples were then assigned into three groups based on their expression levels: low NCAN expression, intermediate NCAN expression and high NCAN expression. NCAN negative samples were not found in our dataset. Examples of the staining intensities are visualized in Figure 9. The evaluation of the staining intensity was done blinded, meaning that no knowledge of the patients clinical or biological data was available

at the time of analyzing the samples. The results were then combined with patients' clinical data and analyzed as described later.

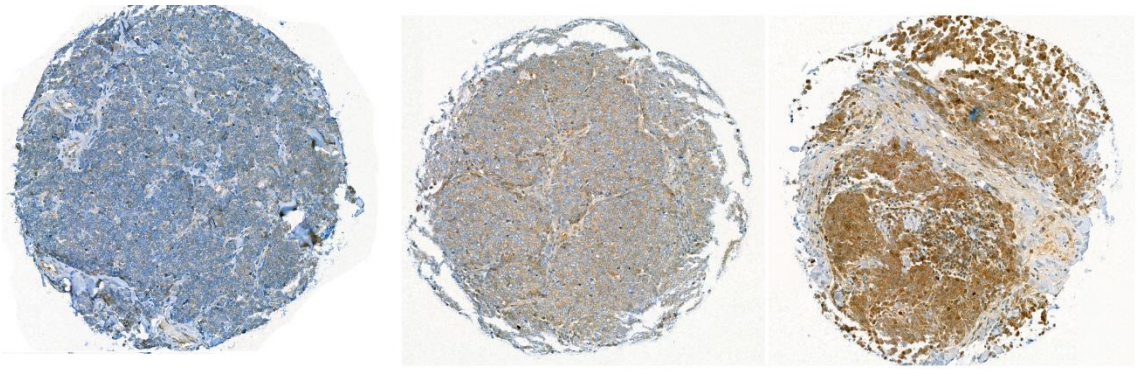

Figure 9. Different NCAN protein expression levels as seen with immunohistochemistry. From left: low, intermediate and high NCAN expression.

Other immunohistochemical markers used in the study, such as large T-antigen (CM2B4), Ki-67 and RB were stained prior to this study and have been described elsewhere (Sihto, Kukko et al. 2011).

Western blotting

Normal cell lines were cultured on 6-well plates (Corning, Greiner bio-one, REF 657160) until they reached ~70% confluence (preparation siRNA protein lysates described later). Protein lysates were extracted from the cells with Pierce™ RIPA buffer (Thermo Scientific, REF 89900) supplemented with 1x HALT™ Protease & Phosphatase Single-Use Inhibitor Cocktail (Thermo Scientific, REF 78442) containing 5mM EDTA (Thermo Scientific, Prod# 1860851). Protein concentrations were analyzed with Pierce™ BCA Protein Assay Kit (Thermo Scientific, REF 23227) using Hidex Sense for absorbance measurements. The lysates were then diluted 1:1 with 2x Laemmli Sample Buffer (Bio-Rad, Cat. #1610737) supplemented with 5% β-Mercaptoethanol and boiled for 10 minutes at 95°C to denature the proteins. Attachment 3 contains the entire western blotting procedure as is described here.

Denatured proteins were then separated from each other with SDS-PAGE gel electrophoresis. The samples were pipetted on a Bio-Rad Mini-PROTEAN TGX gel (Bio-Rad, Cat#4561033) and the gel was placed on BIORAD Bio-Rad Mini Trans-blot cell. A constant voltage (100V) was applied for roughly 1,5 hours to separate proteins based on their molecular weight.

The gel containing the proteins and a Trans-Blot Turbo Transfer Pack (Bio-Rad, Cat. #1704156) were stacked according to manufacturer's instructions and the proteins were transferred onto a PVDF membrane (included in the transfer pack). Bio-Rad Trans-Blot Turbo Transfer System was used for the protein transfer, with a Bio-Rad predefined program (mixed molecular weight, constant 1,3A, 7 minutes). After this, the membrane was taken forward in to the actual western blotting.

Two washes (5 minutes at room temperature) with western blot wash buffer (later called WB, contains 0,1% Tween20 [Thermo Scientific, BP337-100] in TBS) were administered to the membrane prior to blocking non-specific binding of antibodies with the WB supplemented with 5% low-fat milk. The membrane was washed twice as mentioned previously before treating the membrane with primary antibody. For NCAN and MCPyV LT (CM2B4), antibodies from Atlas Antibodies (NCAN, HPA036814), Merck/Sigma Aldrich (NCAN, N0913) and Santa Cruz Biotechnology Inc. (CM2B4, sc-136172) were used at 1:1000 dilution (1% milk in WB). Actin from Bethyl Laboratories (Bethyl Laboratories, A300-491A) was used at 1:100 000 dilution (1% milk in WB) as a housekeeping protein. All of the primary antibodies were incubated over night at +4°C on their own membranes.

The membrane was washed twice as previously, and secondary antibody was applied for the membrane. For Atlas Antibodies NCAN, rabbit-anti-mouse IgG Jackson ImmunoResearch, REF 315-035-003) was applied at 1:10 000 dilution (1% milk in WB), and for Merck NCAN, CM2B4 and Actin, goat-anti-rabbit (Jackson ImmunoResearch, REF 111-035-003) was applied at 1:10 000 dilution (1% milk in WB). All of the secondary antibodies were incubated for 1 hour at room temperature. After this, the membrane was washed twice and a chemiluminescent substrate (SuperSignal West Pico PLUS [Thermo scientific, REF 34580]) was added, and x-ray films were taken from the membranes to visualize the proteins.

Quantitative PCR

RNA samples were extracted from normal and siRNA treated cell lines (described later) with NucleoSpin RNA (Macherey-Nagel, REF 740955.50) kit according to manufacturers' protocols. DNA samples for LT gene copy number (MCPyV status verification) were extracted for another project beforehand (unpublished data). The quality and quantity of the RNA and DNA samples were then measured with NanoDrop 1000 (Thermo Fisher Scientific) spectrophotometer. 100ng of each RNAs were then used as template for cDNA synthesis, performed with iScript cDNA Synthesis kit (Bio-Rad, Cat. #1708891) according to the manufacturers protocol. The cDNA quantity and quality was measured with NanoDrop 1000.

Large T-antigen (LT) gene copy number was studied with Universal ProbeLibrary based qPCR assay, using LightCycler 480 Probes Master kit (Roche diagnostics, REF 04887301001) and Universal ProbeLibrary Set (Roche diagnostics, REF 04683633001) according to the manufacturers' recommendations. This was done to verify the MCPyV status of our cell lines. Protein Tyrosine Phosphatase Receptor Type G (PTPRG) was used as a reference gene. LT and PTPRG primers were designed and are described in more detailed in an article from Sihto et al. (Sihto, Kukko et al. 2009), and briefly in the Appendix 1. Any positive qPCR reaction was considered as a positive finding for MCPyV.

The NCAN and LT mRNA expression levels were studied with SYBR Green (BIO-RAD, SsoAdvanced Universal SYBR Green Supermix, cat no. 1725270) based qPCR assay, with GAPDH as a housekeeping gene. The NCAN primers were

designed with Universal ProbeLibrary Assay Design Center (Roche Diagnostics) and The GAPDH primers were designed for another project (unpublished data) with GETprime (https://gecftools.epfl.ch/getprime). The primers are described further in Appendix 1.

Bio-Rad CFX96 (thermal cycler) and Bio-Rad CFX Maestro (software) were used for the qPCRs. For both of the methods (Universal ProbeLibrary and SYBR Green), a total of 100ng of DNA (MCPyV status) or cDNA template and a final concentration 0,5µM of both forward and reverse primers were used for each reaction. The complete protocols can be found in Appendix 4.

NCAN knockdown with siRNA transfections

Pre-designed ON-TARGETplus siRNAs from Horizon discovery (ON-TARGET-plus Human NCAN siRNA, Catalog ID: L-019794-01-0005) were used to knock-down Neurocan expression in 2 MCPyV+ MCC cell lines (WaGa and MKL1) and 2 MCPyV- MCC cell lines (MCC13 and MCC26). Custom siRNAs targeting large T-antigen (5'-AAGAGAGGCTCTCTGCAAGCT-3') and small T-antigen (5'-AAGTT-GTCTCGCCAGCATTGT-3') were designed in another publication, and provided by Horizon Discovery (Kwun, Guastafierro et al. 2009). ON-TARGETplus Non-targeting Pool (Horizon discovery, D-001810-10-20) was used as a non-targeting control, and siGLO Green Transfection Indicator (Horizon discovery, D-001630-01-05) was used to optimize the siRNA transfection conditions. Lipofectamine 2000 and 3000 (Invitrogen, REF 11668-019 and REF L3000-015 respectively) transfection reagents were tested for optimal transfection capability, and Lipofectamine 2000 was eventually used in the knockdown assays.

For protein and RNA lysates 100 000 cells for MCC13 and MCC26, and 400 000 cells for MKL1 and WaGa cell lines were plated on 6-well plates (Greiner bio-one, REF 657160). For cell proliferation assays 10 000 cells for MCC13 and MCC26, and 20 000 cells for MKL1 and WaGa cell lines were plated on a 96-well plate (Corning, 3596). For both experiments, cells were counted and plated in growth media on day 0. On day 1, cells were transfected with siRNAs (final concentration 75 nM) using 0,33 µl/well or 6 µl/well of Lipofectamine 2000 for 96-well plate and 6-well plates respectively. First, a mixture of Lipofectamine 2000 and target (or control) siRNA was prepared in Opti-MEM (Gibco, REF 31985-047) and incubated in room temperature for 5 minutes, as per manufacturers' instructions. The following mixture was then applied to cells, and the cells were grown for 0-72 hours, depending on the experiment. For protein and mRNA lysates, cells were grown for 72h where as for cell proliferation studies, 3 different time points were used: 0h, 48h and 72h. After the incubation, the lysates were prepared as described previously, or the cell proliferation was measured as described next.

Cell proliferation with CellTiter-GLO

Cell proliferation was measured with CellTiter-GLO Luminiscent Cell Viability Assay (Promega, Cat. #G7571/2/3). Briefly, the assay is based on ATP catalyzed

reaction where luciferin is transformed into oxyluciferin. In the process, a luminescent signal will be produced. Since ATP is produced by living cells, the amount of luminescent light will correlate with the number of living cells in a sample.
MCC cell lines were transfected with siRNAs as described previously. Transfected cells were grown for three different time points: 0, 48 and 72 hours. After this, premade CellTiter-GLO reagent was added to the cells following the manufacturers' instructions, and the luminescence was measured with Hidex Sense. Due to a mistake in the experimental setting, complete data is available only from MKL1 and WaGa cell lines. The MCC13 and MCC26 experiments were scheduled after the MCPyV positive cell lines, but due to the recent outbreak of COVID-19 pandemic, this could not be fitted into the thesis timeframe.

Statistical analysis

All statistics were analyzed with either IBM SPSS Statistics 25 or Rstudio version 1.2.5033. Apart from the bioinformatics data that was provided by MediSapiens ltd., all of the statistics have been analyzed and visualized by the author.

Results

Identification of NCAN

141 RNA samples were sequenced, out of which 111 (79%) had good enough quality to be processed further in the bioinformatics pipeline. The gene expression was derived from the samples with deseq2 and further on the outlier genes were detected from the deseq2 data with multiple different detection methods: SIBER, GTI, ranked gene list (deseq2 based, MCPyV+ vs MCPyV- cases) and IST ranking. We focused on finding interesting genes that were visible in multiple outlier detection methods. This was achieved by comparing the HUGO Gene Nomenclature Committee (HGNC) identification codes of the genes listed in the different methods with RStudio (version 1.2.5033, R package 3.5.2) using the merge() function. Figure 10 represents the found outlier genes as a VENN diagram. This was further compared to outlier genes detected between MCC subtype specific outliers also compared with the merge() function, visualized also in Figure 10.

After obtaining a list of suitable and interesting genes, few selected genes were manually scrutinized in multiple online databases such as OMIM, DGIdb and IST online. Neurocan was chosen as our protein of interest, as it showed potential as a biomarker separating MCPyV+ and MCPyV- cases based on the SIBER, ranked gene list, GTI and hierarchical clustering of top 100 variance genes arranged for the parent project. It also seemed to be slightly misplaced, since it should be found mainly in central nervous system, and while MCC is considered neuroendocrine tumor, Neurocan over/under expression has not been reported previously on other neuroendocrine, non-CNS tumors. Normal tissues outside of

the central nervous system have low Neurocan expression as displayed by Figure 11 and the same applies for various cancerous tissues, as visualized by Figure 12.

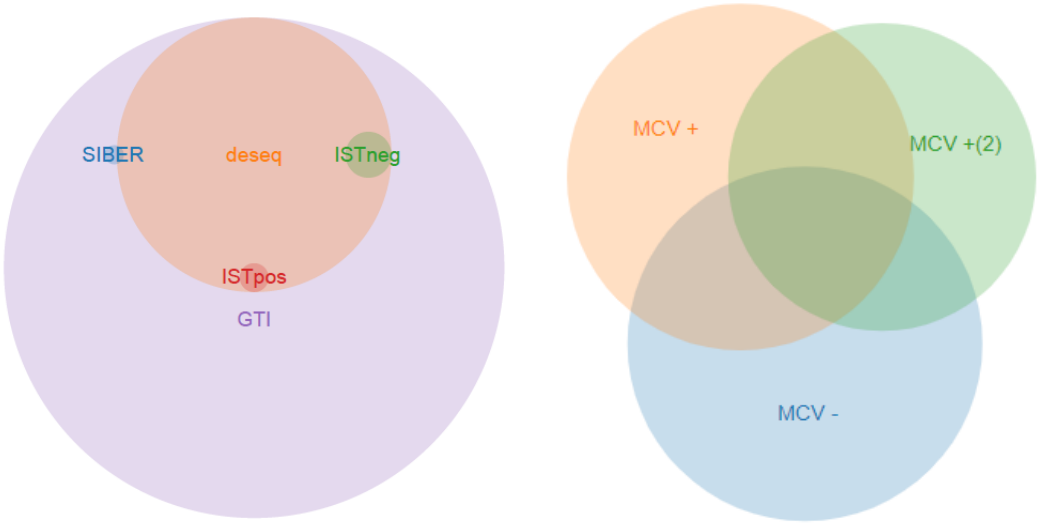

Figure 10. VENN diagrams of HGNC id distribution when comparing outlier gene detection methods and MCC subtypes by HGNC ids. SIBER = SIBER outlier gene detection method, deseq = ranked gene list, MCPyV+ vs MCPyV- cases, IST pos = IST-ranking, MCPyV+ cases, IST neg = IST-ranking, MCPyV- cases, GTI = Gene tissue indexing.

A	SIBER	IST neg	IST pos	Ranked gene list	GTI
SIBER	19	0	0	6	19
IST neg	0	112	0	112	112
IST pos	0	0	44	44	44
Ranked gene list	19	112	44	4031	4031
GTI	19	112	44	4031	13400

B	MCPyV+	MCPyV+ (2)	MCPyV-
MCPyV+	4388	1963	1835
MCPyV+ (2)	1963	3459	1521
MCPyV-	1835	1521	4588

Table 2. Number of genes in different gene outlier detection methods and their overlap. B) Number of differently expressed genes in each subtype compared to each other, and their overlap.

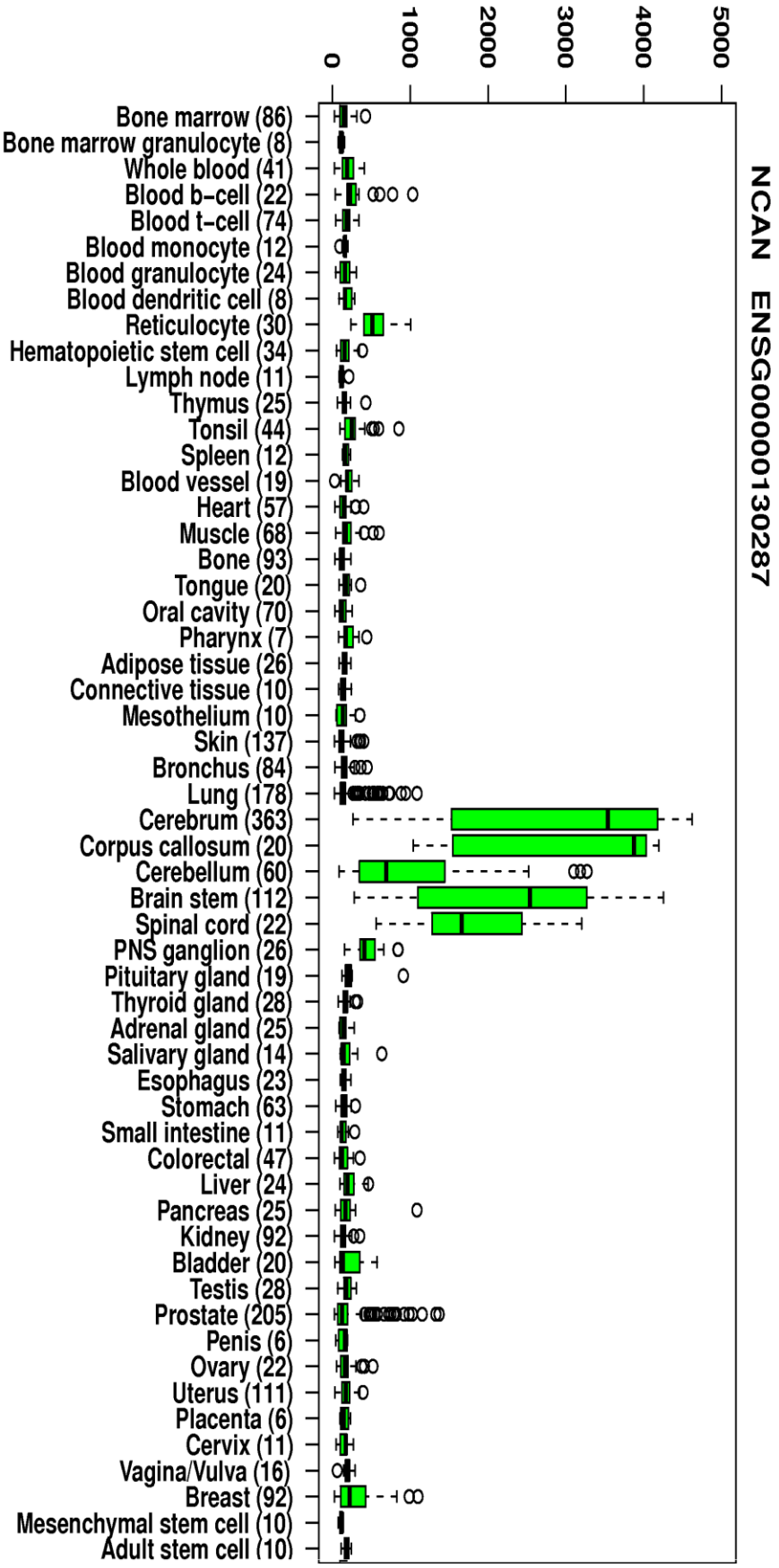

Figure 11. Neurocan expression in various healthy tissues (MediSapiens ltd. 2011).

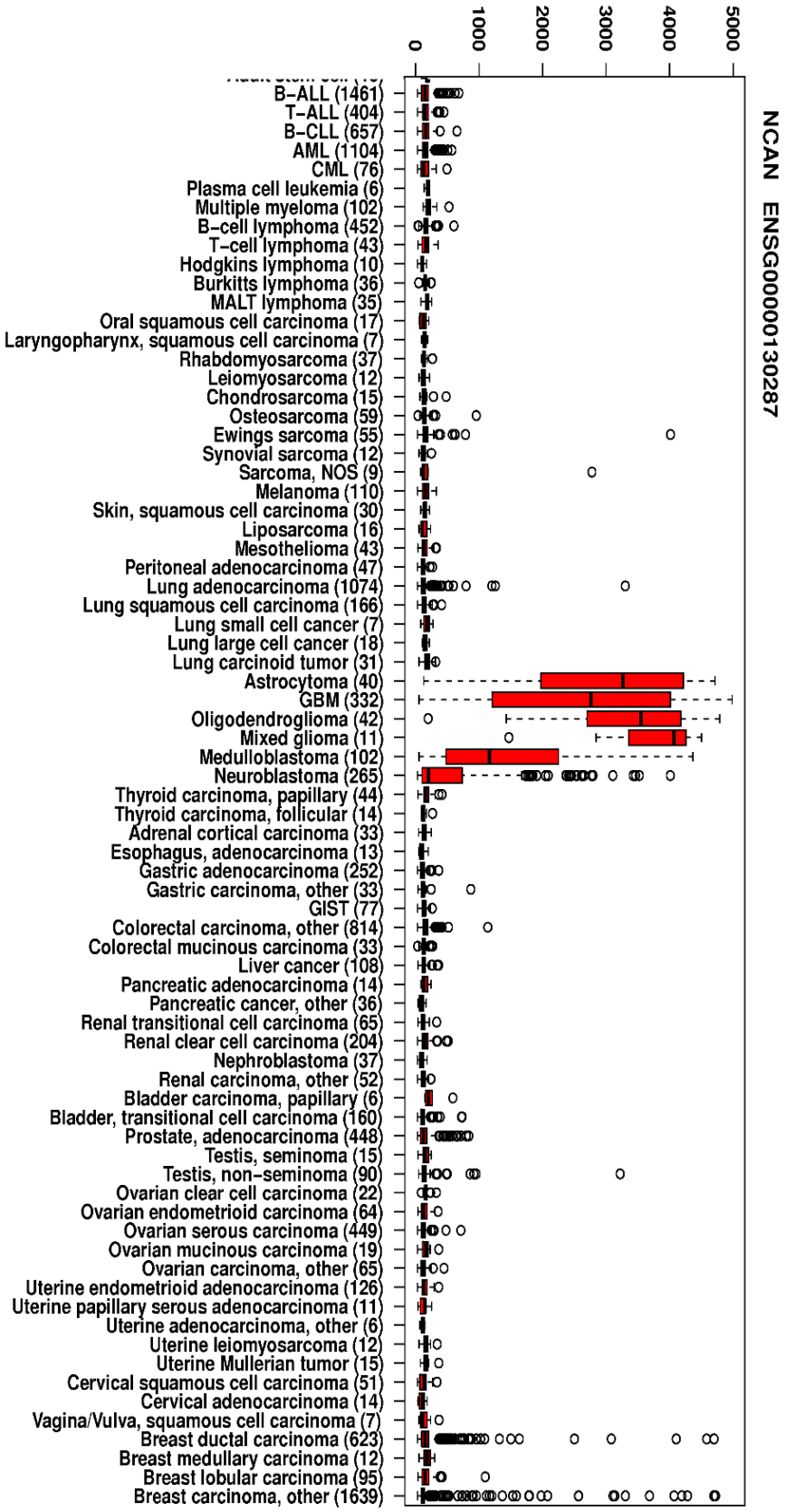

Figure 12. Neurocan expression in various tumors (MediSapiens ltd. 2011).

When comparing the gene expression levels of MCPyV+ and MCPyV- tumors, Neurocan ranked 21st in the deseq2 based ranked gene list. GTI analysis supported the hypothesis of differential expression; however, this was statistically not significant. SIBER analysis provided much needed insight and visualized the Neurocan expression in MCPyV+ versus MCPyV- tumors as displayed in Figure 13.

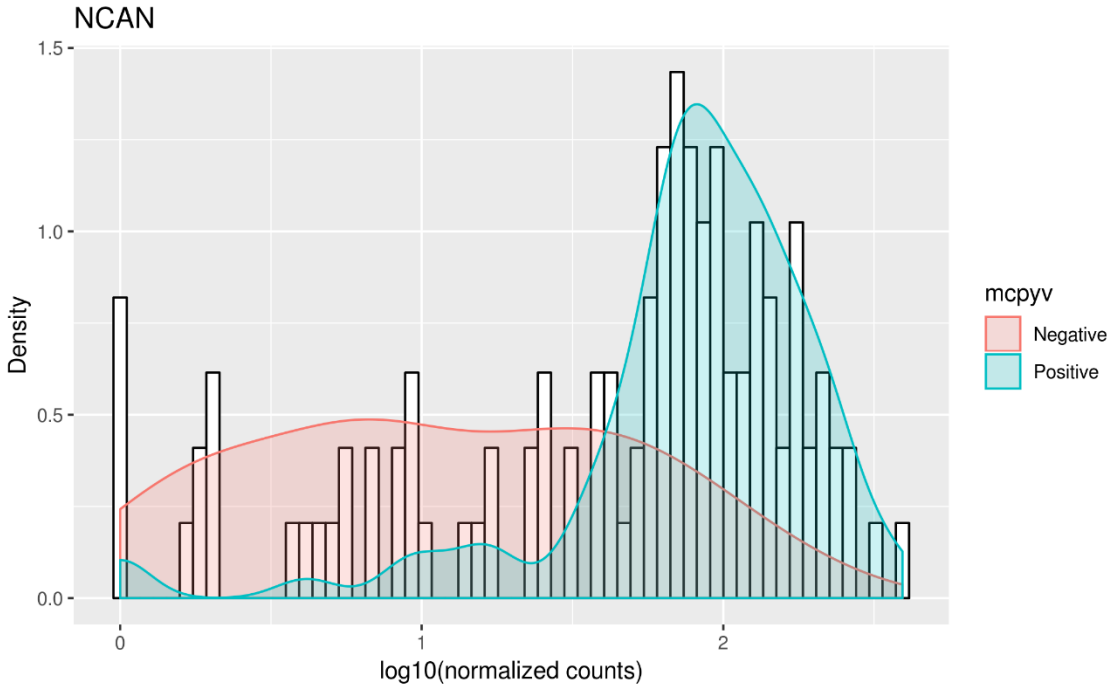

Figure 13. SIBER analysis of Neurocan expression in MCPyV+ vs MCPyV- samples.

The x-axis of the SIBER analysis represents the expression of NCAN in a given sample while the y-axis represents the number of samples. This gives us an overall expression profile of the samples, and when stratified with MCPyV status, we can see that MCPyV positive samples tend to have a higher overall expression of NCAN.

Immunohistochemistry

To confirm the bioinformatics findings of the differential expression, TMAs from the MCC sample series were immunohistochemically stained for Neurocan protein. 144 samples were stained and grouped into three categories based on the level of staining: low Neurocan expression (31 cases), intermediate Neurocan expression (60 cases) and high Neurocan expression (53 cases). Out of the 144 samples 144 had survival data available (41 MCC related deaths) and 125 had MCPyV status identified. As described in Figure 14, in the low NCAN expression group 12 cases (54,5%) were MCPyV negative and 10 cases (45,5%) were MCPyV positive, in the intermediate group 17 cases (30,4%) were MCPyV negative and 39 cases (69,6%) were MCPyV positive and in the high expression group 8 cases (17%) were MCPyV negative and 39 cases (83%) were MCPyV positive.

This shows that there is an association in the cross tabulation, with high NCAN expression correlating with the MCPyV positive cases, where as low NCAN expression correlates with MCPyV negative cases. Pearsons chi-square test shows that this is a significant finding at a level of p=0.006. Taken together, these results confirm that there is a significant association between NCAN expression and MCPyV status, with low NCAN expression correlating with MCPyV negativity and vice versa.

NCAN expression versus MCPyV status

			MCPyV status	
			Negative	Positive
NCAN expression	Low	Count	12	10
		%	54,5%	45,5%
	Intermediate	Count	17	39
		%	30,4%	69,6%
	High	Count	8	39
		%	17,0%	83,0%
Total		Count	37	88
		%	29,6%	70,4%

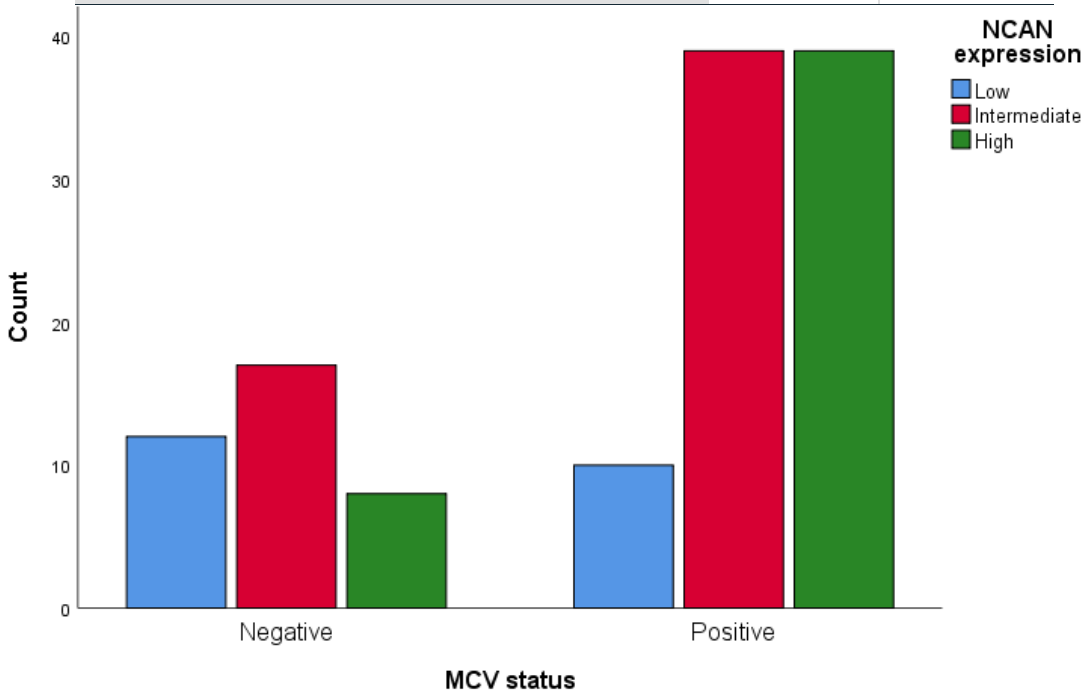

Figure 14. NCAN expression versus MCPyV status crosstabulation. Neurocan expression is divided into 3 groups, low, intermediate and high.

Next, we analyzed the effect of different NCAN expressions in patient survival. Kaplan-Meier method was used to analyze the differences between low, intermediate and high NCAN expression groups. As shown in Figure 15, there is a clear difference in MCC specific survival between the low NCAN expression group and

the two other groups (p-value = 0.044). When looking at overall patient survival, the story remains the same; low NCAN expression is associated with worse prognosis (Figure 16). This is not surprising, as we have shown low NCAN expression associates to MCPyV negative MCC subtype, which has a worse prognosis than MCPyV positive subtype (Sihto, Kukko et al. 2009). Other clinical factors, patient age (p-value = 0.18), tumor size (p-value = 0.64), gender (p-value = 0.49), cancer stage (p-value = 0.63), location of the primary tumor (p-value = 0.25) and metastasis at the time of diagnosis (p-value = 0.89), had no significant association with NCAN expression levels.

It should be noted, that minimal data censoring was applied to the data, as the dataset that we had at our disposal is relatively small. Data censoring would in this case result in subgroups becoming too small to be statistically relevant. For example, if we censor all cases that lack MCPyV status and cases that have metastasis at the time of diagnosis (often censored as these patients have poor prognosis by default and could cause skewness in statistical analysis), or have this information missing, the amount of cases in MCPyV negative/high NCAN expression group would be limited to 4 cases. This hinders our ability to produce statistically reliable results. However, we understand that not censoring the data with certain parameters, such as metastasis at time of diagnosis, is going to affect the results, yet we decided that this is acceptable in the frame of this master's thesis due to the limited sample size and time available.

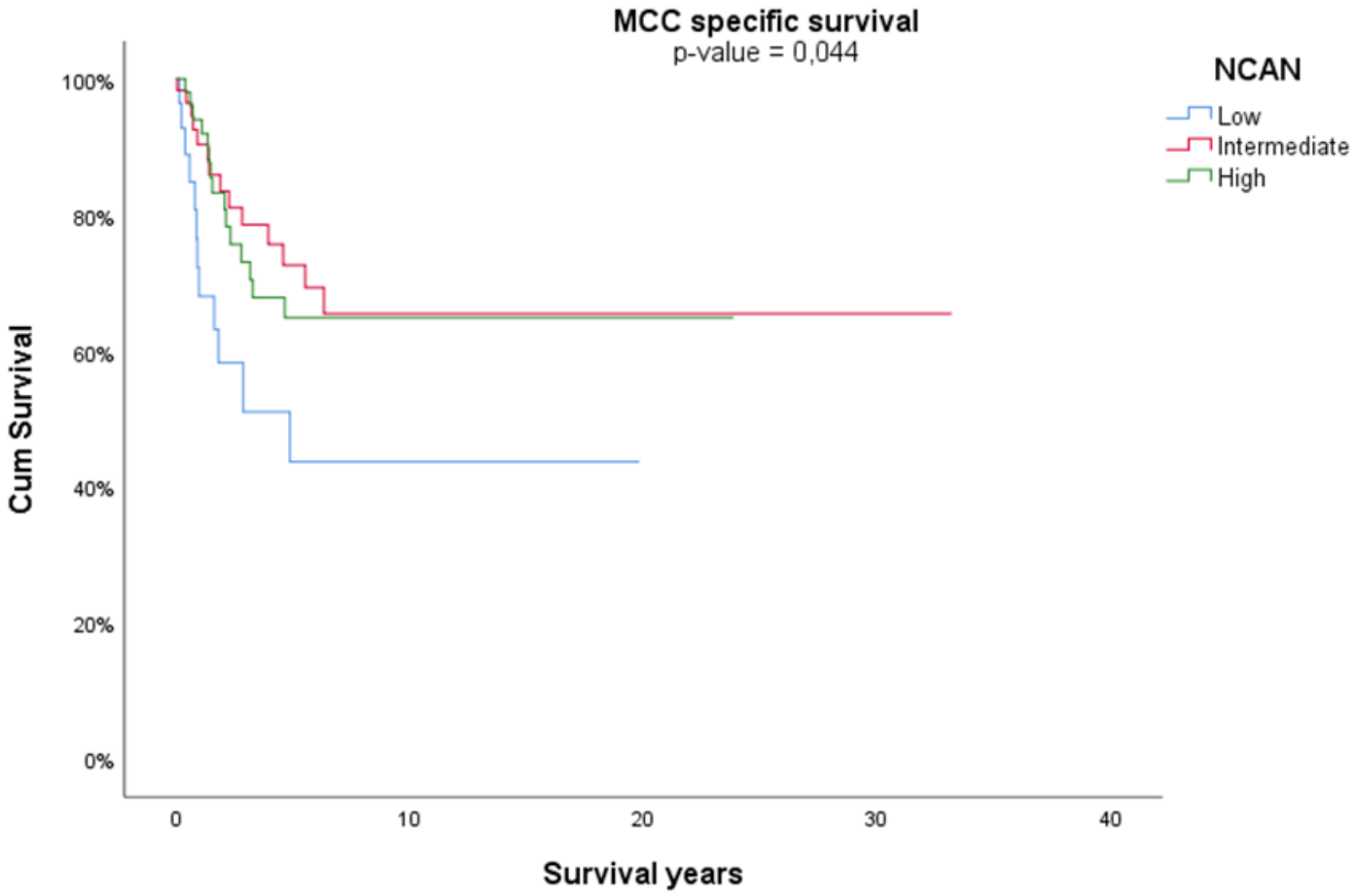

Figure 15. MCC specific survival. Kaplan-Meier survival analysis.

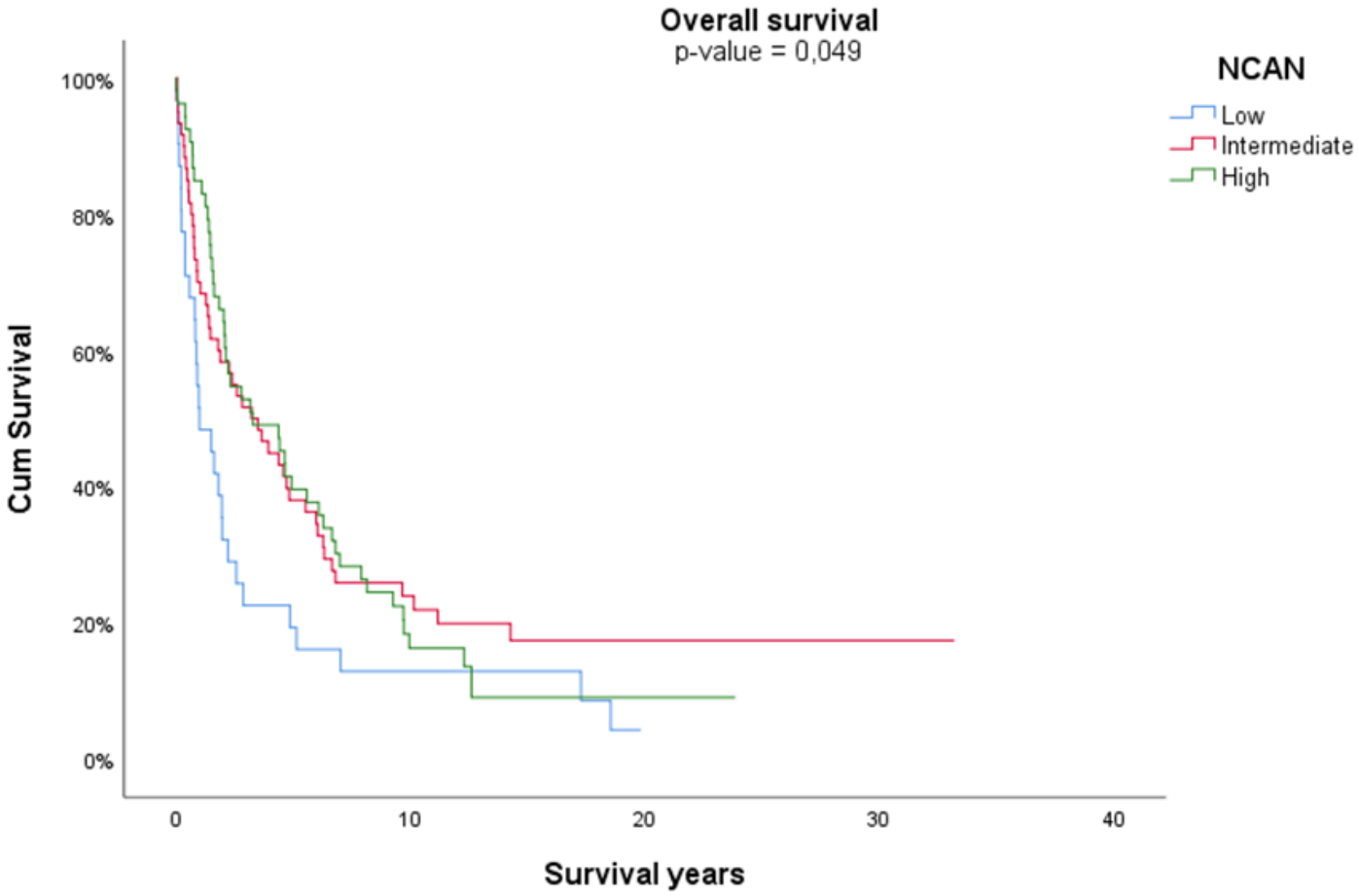

Figure 16. Overall patient survival. Kaplan-Meier survival analysis.

Next, we analyzed whether NCAN is an independent variable causing the difference in patient prognosis. Cox proportional hazard model of different NCAN expression levels showed that low NCAN expression group had a 2.2 times higher hazard ratio (95% confidence interval: 1.03-4.7) compared to the reference group (high NCAN expression). However, this model was not statistically significant, possibly due to small data size, or high variance in survival in each group.

When MCPyV status was added to the model, NCAN expression lost its significance. This leads us to believe that NCAN related survival differences are indeed somehow connected to MCPyV (Figure 18). However, we can see the downside of working with a rare cancer clearly in these models. Achieving statistical significance is extremely difficult as the number of events (in this case, number of patients who died to MCC) is only 33. For a multivariate analysis like Cox proportional hazards, this is a small amount. However, a significant result in a small dataset like these, is usually a promising sign and indicates that larger studies/datasets could be justified.

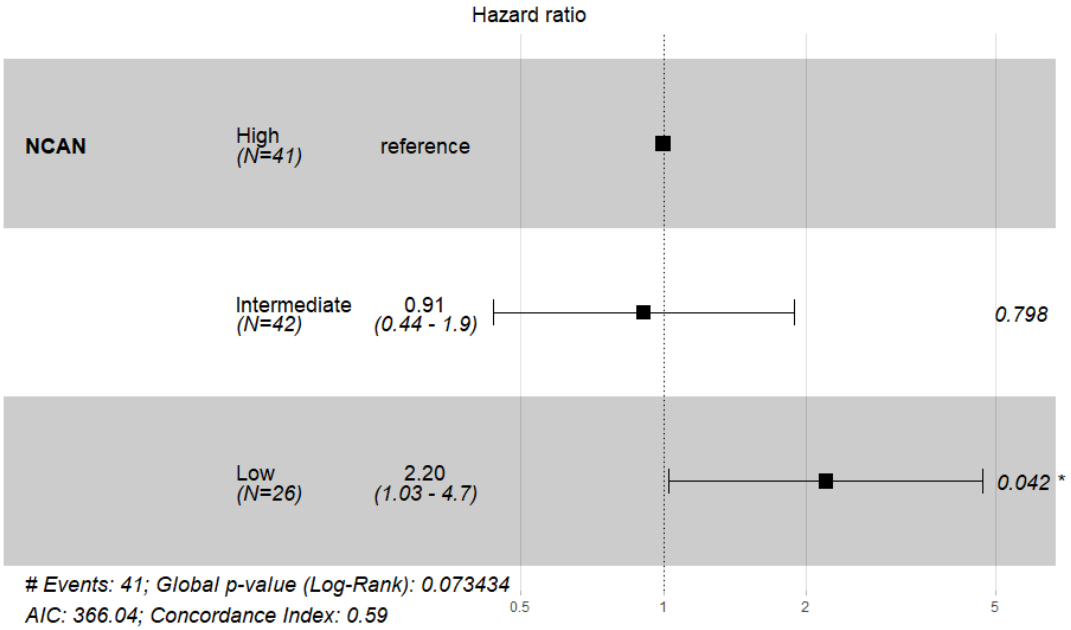

Figure 17. Cox proportional hazards regression model, MCC specific hazards, NCAN expression levels.

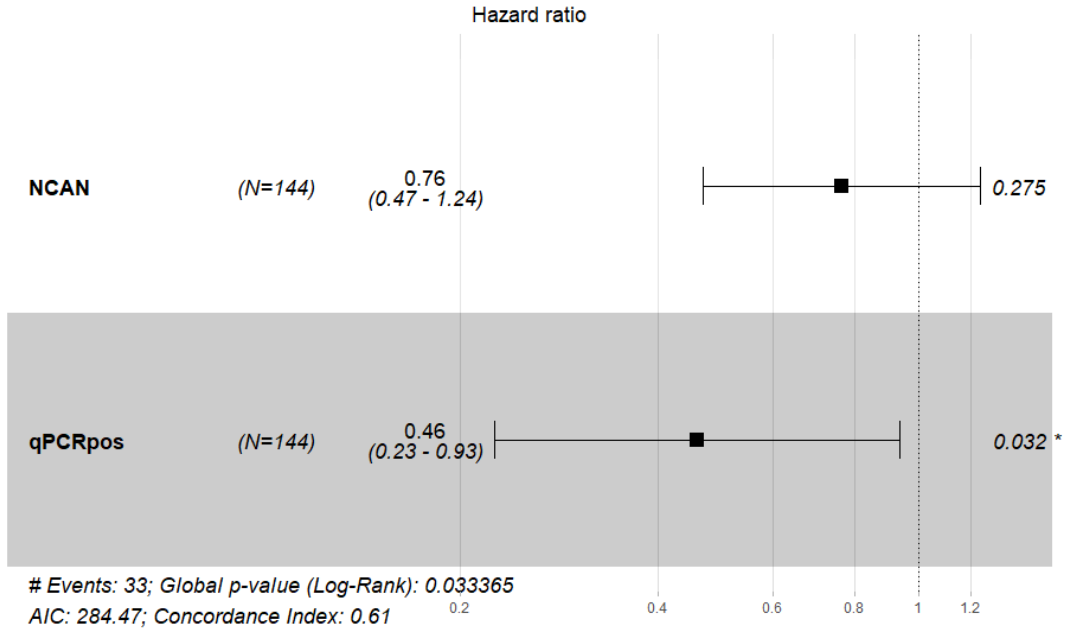

Figure 18. Cox proportional hazards regression model of NCAN and MCPyV status, MCC specific hazards.

Moving on to a larger scale model, the small sample size started to provide significant challenges. Only clinical variables that were prognostic factors in univariate models (Kaplan-Meier) were added to the model. For example, age at the time of diagnosis was not a prognostic factor in our MCC sample series, and was thus not added to the model. To add the cancer stage to the analysis, we had to combine stage 3 and 4 cancers (stage 3 = local metastasis, stage 4 = distant metastasis/systemic disease), to achieve statistically relevant sample size for the groups (n=12 when combined). Other clinical variables (tumor size, patient gender and primary tumor location) were added as they were.

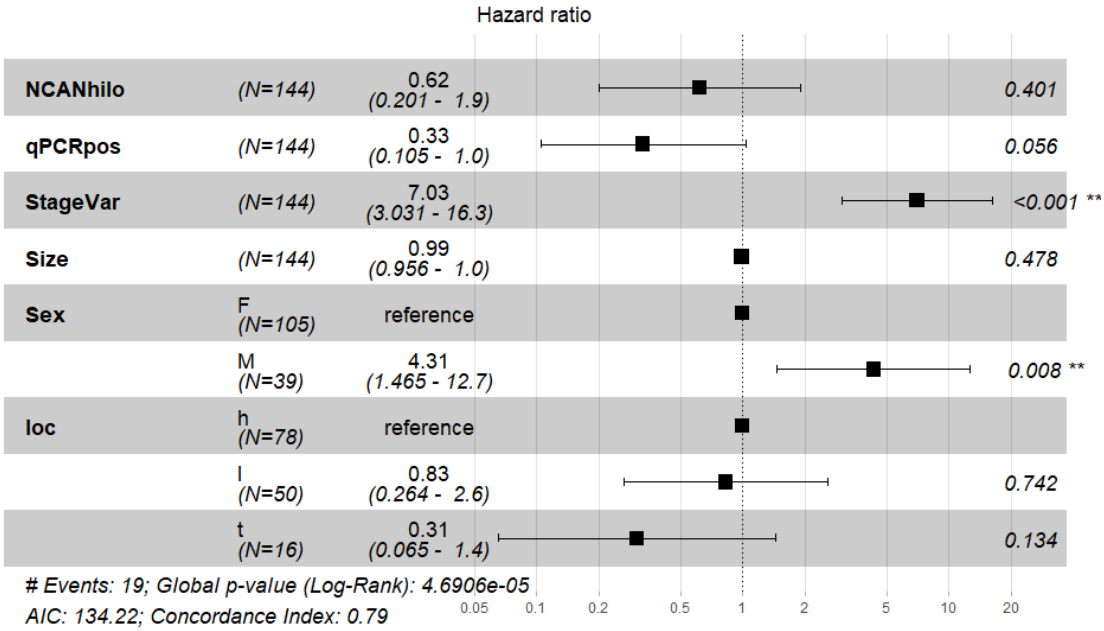

Figure 19. Cox proportional hazards regression model, MCC specific hazards, multiple variables. F=female, M=male, loc=location of primary tumor, h=head and neck, l=limb and t=torso.

It is clear that cancer stage is one of the hazardous factors in MCC specific survival. The other significantly hazardous factor in our model is the sex, with male gender having 4.31 (95%CI 1.465-12.7) times higher risk to die of MCC compared to females. Other variables of interest have lost their significance in the model. This hazard model needs to be expanded with additional data to increase its reliability, and biological variables such as cell proliferation marker Ki-67 should be added. While much of the data already exists in the dataset at our disposal, it is too fragmented to be used, and requires updating. However, the timeframe of this thesis is too short for this sort of maneuvers. This will be looked into in depth in the discussion section.

When applying the models to overall survival, the story remains the same. However, the number of events and also the number of samples overall increased to acceptable sizes. Interestingly, the global p-value for the model remains statistically not significant in case of NCAN expression only and NCAN and MCPyV status combined. This implies that the variation in one of these variables is exceedingly high. This is probably due to NCAN expression levels high and intermediate, which in the Kaplan-Meier survival analysis show similar prognosis for the patient, but in the eyes of a statistical analysis are represented the wrong way round as intermediate expression has marginally better prognosis. Indeed, if we combine these groups and focus on studying only low NCAN expression versus intermediate and high combined, we see that the model only containing NCAN expressions becomes statistically significant (Figure 21). However, the effect is only marginal and does not transfer into the larger models (data not shown).

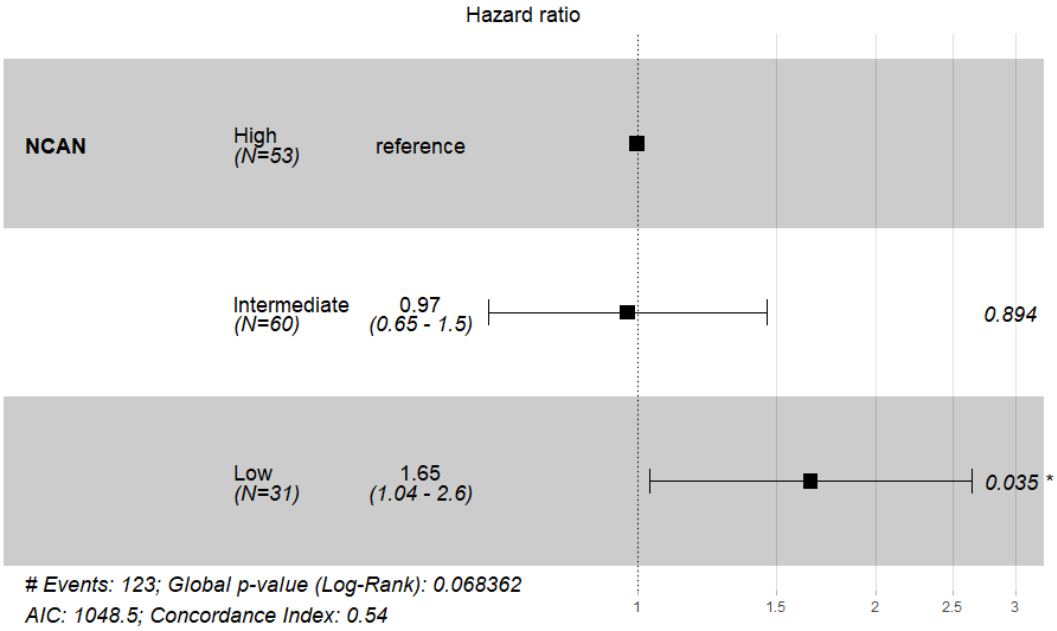

Figure 20. Cox proportional hazards regression model, overall hazards, NCAN expression.

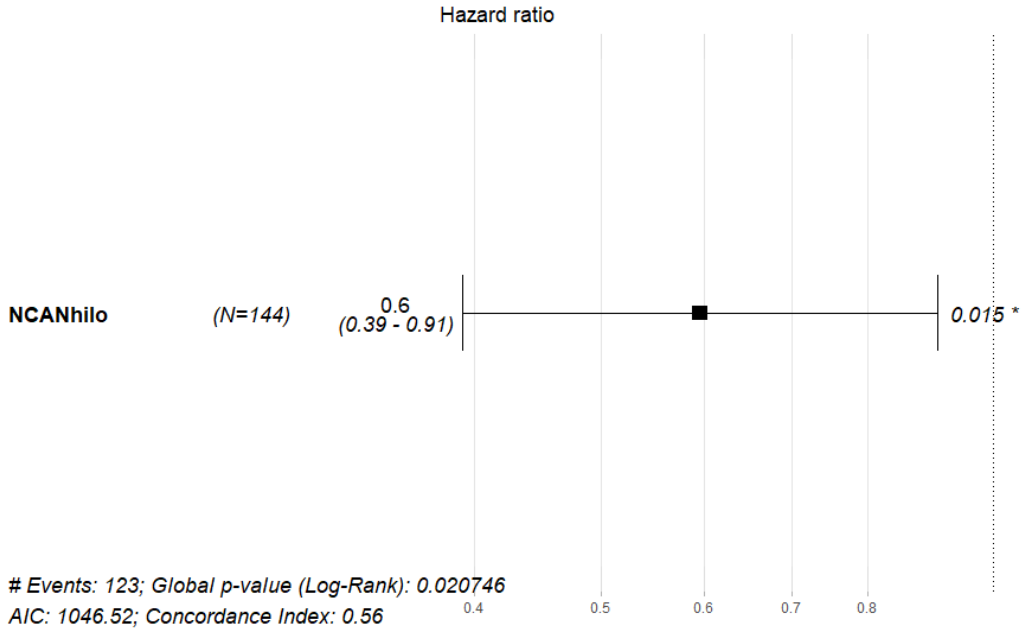

Figure 21. Cox proportional hazards regression model, overall hazards, low NCAN expression versus combined intermediate and high NCAN expression.

Once again, the NCAN expression loses its significance when other variables are added to the model. Interestingly the global p-value for NCAN and MCPyV status model remains non-significant even after combining the two groups as previously described (data not shown). However, when including the rest of the clinical variables, the model is highly significant (p-value < 0.01), and we can see that the only two significant variables contributing to the overall hazard (in this model) are the MCPyV status and cancer stage.

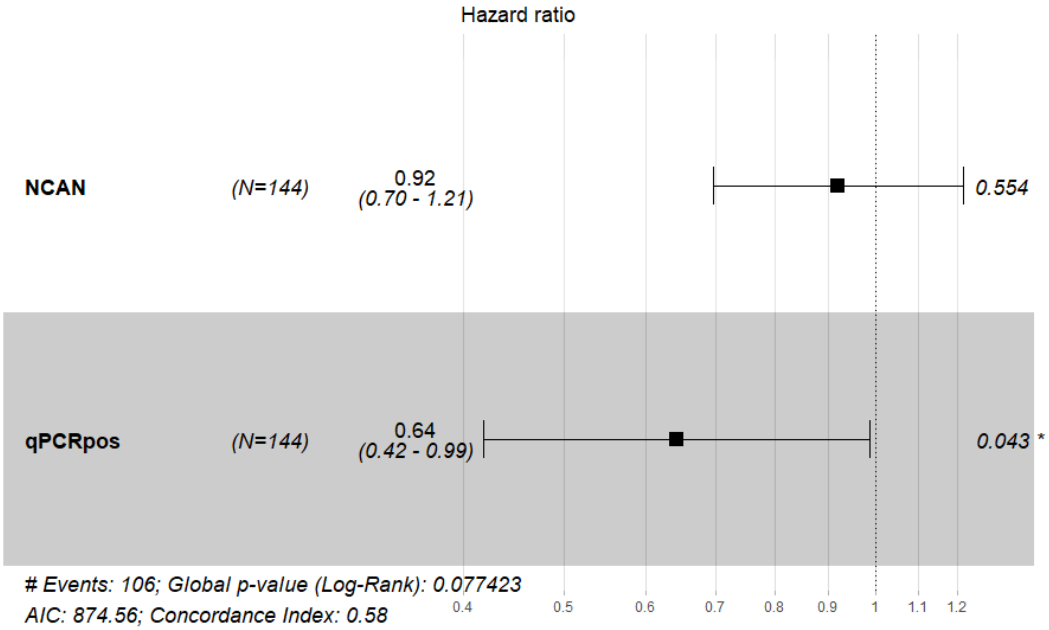

Figure 22. Cox proportional hazards regression model, overall hazards, NCAN and MCPyV status.

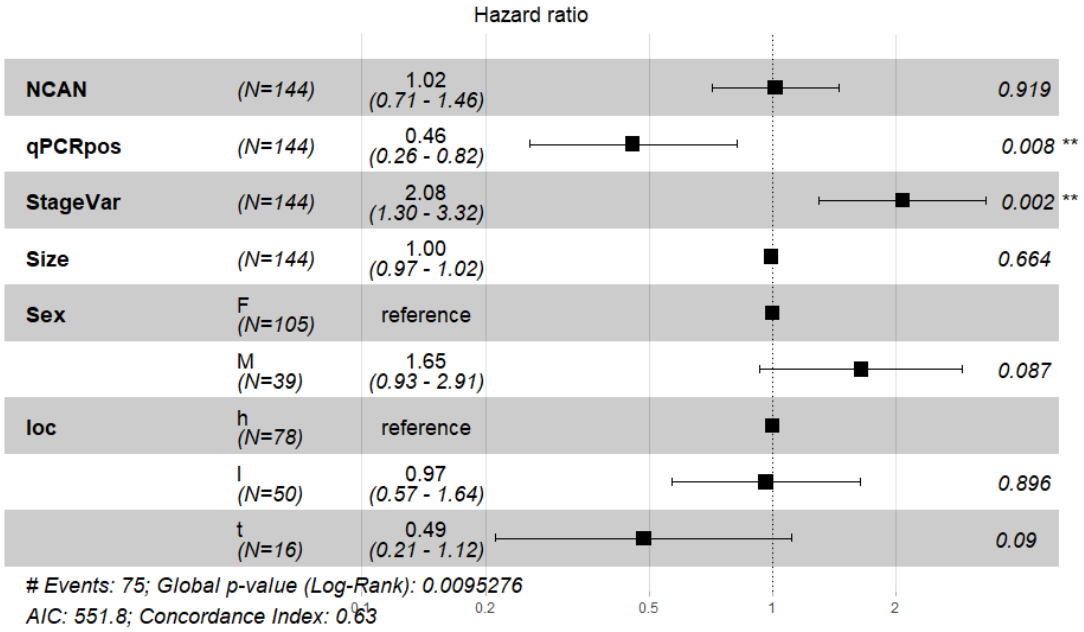

Figure 23. Cox proportional hazards regression model, overall hazards, multiple variables. F=female, M=male, loc=location of primary tumor, h=head and neck, l=limb and t=torso.

Overall, the Cox proportional hazards regression tells us a few things. Firstly, NCAN is not an independent variable when it comes to patient survival, and it is more likely functioning through MCPyV T-antigens or a common factor yet unknown. Secondly, the dataset at our disposal needs to be further expanded and normal biological variables such as Ki-67, p53 and Rb should be incorporated to this hazard model to achieve its full potential.

NCAN expression levels in MCC cell lines

We first verified the MCPyV status of our cell lines with qPCR from DNA samples extracted from our cell lines prior to this project. The qPCR was performed with Roche Universal ProbeLibrary based assay. PTPRG was used as a reference gene and the MCPyV status was derived with LT3 (Large T-antigen transcript number 3). The list of primers used, and the protocol for the qPCR can be found in appendix 1 and 4, respectively. For all of the qPCR reactions, triplicate samples for each cell line were used.

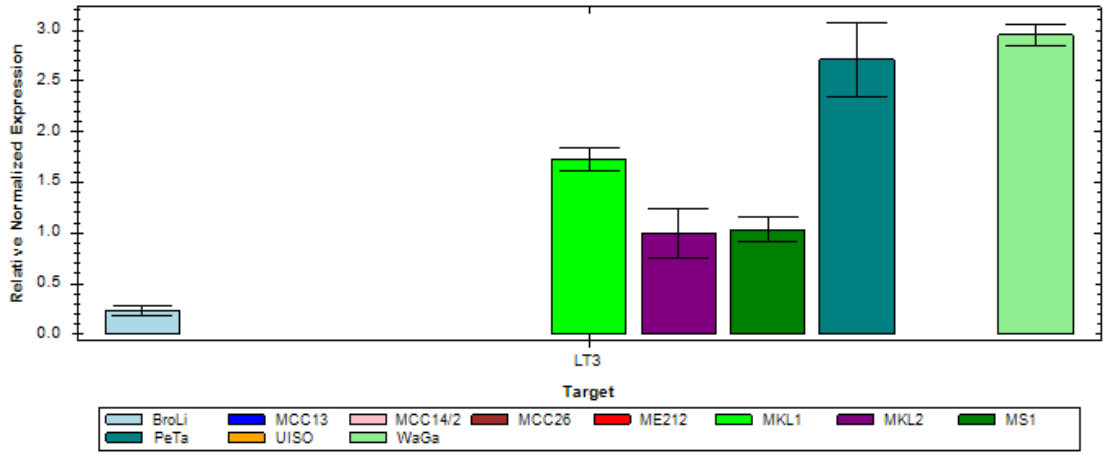

Figure 24. MCPyV status of MCC cell lines. A positive qPCR result equals MCPyV positivity.

The results are in line with pre-existing data, and confirm the MCPyV status of our cell lines. Next, we analyzed the NCAN mRNA expression levels of our MCC cell lines with Bio-Rad SYBR Green based assay with GAPDH as a housekeeping gene. The full protocol can be find in appendix 4. UISO and ME212 cell lines were excluded from further studies. UISO is a controversial MCC cell line as it does not resemble other MCCs, and its origin has been questioned. ME212 cell line has just been recently established and is still in a state of unstable growth. Thus the results might not be replicable, nor comparable to the other cell lines.

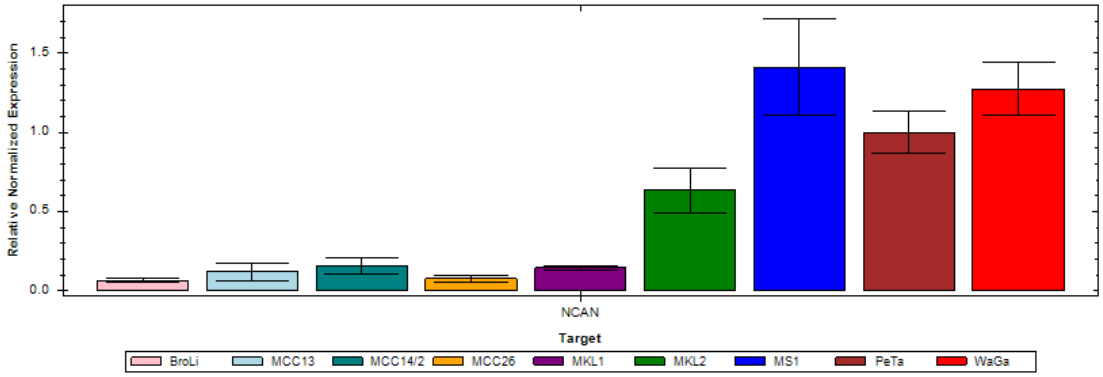

Figure 25. NCAN mRNA expression in MCC cell lines. GAPDH used as reference gene.

Figure 25 would imply that there are differences in NCAN mRNA expression levels between different MCC cell lines. Furthermore, it would seem that MCPyV positive cell lines have higher NCAN mRNA levels than MCPyV negative cell

lines, as is the case in MCC patient samples. Indeed, when we analyzed the NCAN expression differences between MCPyV positive and MCPyV negative cell lines with Student's t-test, we see that there is a statistically significant difference between these two groups (Table 5), when assuming that the variances between the groups are not equal, as indicated by Levene's Test for Equality of Variances (Table 4).

Group Statistics

	MCPyV status	N	Mean	Std. Deviation	Std. Error Mean
Normalized Expression	Negative	3	3,86E-05	1,35E-05	7,78E-06
	Positive	6	2,47E-04	1,87E-04	7,64E-05

Levene's Test for Equality of Variances

F	Sig.
9,937	0,016

Table 3. Group statistics of NCAN expression qPCR and Levene's test for Equality of Variances in Student's t-test, MCC cell lines. Null hypothesis (variances between MCPyV positive and negative groups are equal) is rejected with a p-value of 0.016.

To be noted, the sample size for both groups is very low (n=3 for MCPyV negative cell lines), and more samples would benefit the analysis greatly. Additional MCC cell lines are however, scarce and not available during the timeframe of this project.

Independent Samples Test

		t-test for Equality of Means						
		t	df	Sig. (2-tailed)	Mean Difference	Std. Error Difference	95% Confidence Interval of the Difference	
							Lower	Upper
Normalized Expression	Equal variances assumed	-1,866	7	0,104	-2,09E-04	1,12E-04	-4,73E-04	5,57E-05
	Equal variances not assumed	-2,721	5,103	0,041	-2,09E-04	7,67E-05	-4,05E-04	-1,27E-05

Table 4. Student's t-test of MCC cell line NCAN expression levels. MCPyV status versus NCAN normalized expression levels.

We next moved on to measuring the protein levels of both NCAN and MCPyV in the cell lines with western blotting as described previously. We first used antibodies from Atlas Antibodies for NCAN and Santa Cruz for MCPyV T-antigen. The NCAN antibody seemed at first to be working; however, closer inspection revealed that there were no bands of the expected size visible. For the CM2B4

antibody, we were already aware that there are no commercial MCPyV T-antigen antibodies, that would be of good quality, not to mention interpretable. This proved to be the case later on when we got to silencing the genes with siRNAs, more of which later on. At the end, we chose to go further with the CM2B4 antibody and for the NCAN, we decided to try another antibody from Merck/Sigma Aldrich, that was ordered on accident and is specific for rat NCAN. However, as rat NCAN G1 and G3 domains share 92% homology (G2 domain 29%) with human NCAN, we decided to try the antibody with our samples. However, the results were similar to the previous ones (data not shown).

Figure 26. NCAN (Atlas Antibodies) western blot with MCC cell lines. Bands (cell lines) from left to right: MKL1, MS1, MKL2, MCC13, MCC14/2, MCC26, BroLi, PeTa, WaGa.

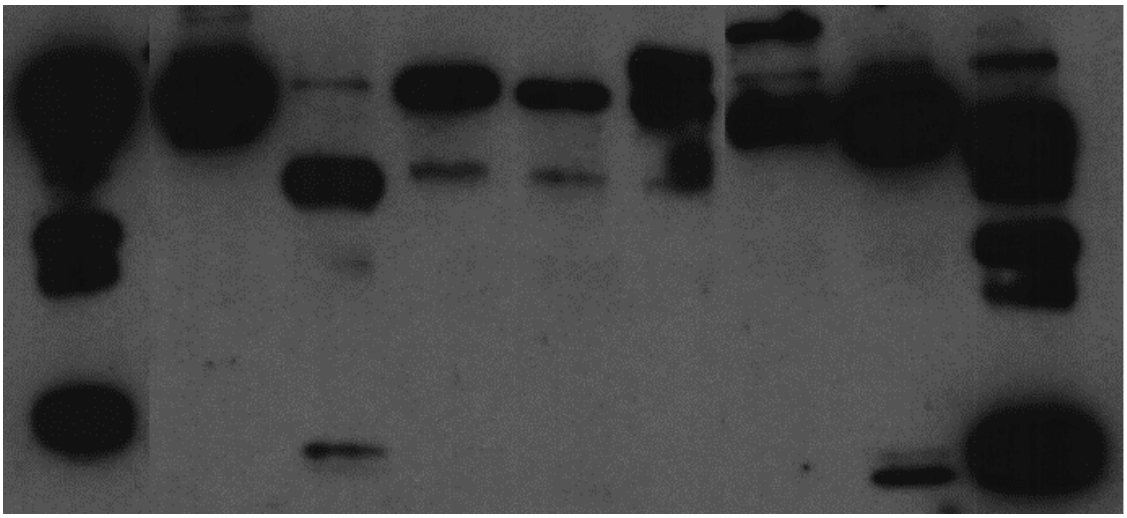

Figure 27. CM2B4 (Santa Cruz) western blot with MCC cell lines, MCPyV status (+ or -) indicated in brackets. Bands (cell lines) from left to right: MKL1 (+), MS1 (+), MKL2 (+), MCC13 (-), MCC14/2 (-), MCC26 (-), BroLi (+), PeTa (+), WaGa (+).

As is visible from Figures 26 and 27, the “protein levels” visualized with western blots do not correlate with the ones deduced from mRNA levels. Cytoskeletal actin was used as a housekeeping protein (data not shown) to verify that equal amounts of total protein lysates was applied from each cell line. Some possible reasons why the NCAN western blots did not work as hoped are further discussed later in this thesis, however, the western blots and thus the cell line protein levels of NCAN was deemed indecisive. For the MCPyV LT, we can clearly see that the specificity of the antibody is not optimal. While the specificity could have been improved, the timeframe of the thesis was too narrow for further optimization. While these results can not be used to tell the MCPyV status of the cell lines by themselves, we hoped that this level of specificity would have been enough for visualizing changes in mRNA expression levels after siRNA treatment.

siRNA knockdown of NCAN and MCPyV T-antigens

Two MCPyV negative and two MCPyV positive MCC cell lines were picked for the siRNA studies: MCC13 (-), MCC26 (-), MKL1 (+) and WaGa (+). While there would have been cell lines with higher NCAN expression (based on qPCR results) and thus possibly more potential for the studies, we tried to incorporate cell lines that would have variation in their characteristics and would be easy to work with. MCC13 and MCC26 are both MCPyV negative cell lines and grow as an adherent monolayer, where as MKL1 and WaGa are MCPyV positive cell lines and grow as suspension cells; MKL1 in big spheroid like clusters and Waga as a single cell suspension. Working with all of the cell lines would have been too time consuming in the available timeframe, and we wanted to incorporate all of our cell lines to the siRNA studies in the future. This includes cell lines that are extremely slow to grow (BroLi) and cell lines that were not in a ready state at the time of these experiments (ME212).

Prior to the actual siRNA studies, we optimized siRNA transfection protocol to our best extent. siGLO, a non-targeting siRNA tagged with GFP protein, was used in the optimization process. Two different transfection reagents were tested, Lipofectamine 2000 and Lipofectamine 3000, and Lipofectamine 2000 proved to be more suitable for these cell lines. To note, there are many other options for transfection reagents, however, these are the ones that we are familiar with and have provided reliable transfection results in our previous experiments. A total of 7 different siRNA (siGLO) concentrations were tested (20,40,50,60,75,80 and 100 nM) in two optimization rounds, and 75nM final concentration was decided to be the best compromise between inducing unspecific cell death and achieving proper transfection rates.. Appendix 5 shows a few examples of the transfection efficiency during the optimization steps.

As described previously, the siRNA transfections lasted for 72 hours for the lysates (both protein and RNA), where as the cell proliferation assay had three time points 0h, 48h, and 72h. Next we will go through these results individually.

RNA and protein levels after siRNA knockdown

We first looked at the RNA level changes resulting from the siRNA knockdown. For MKL1 the transfection seems to have worked nicely, with relative normalized mRNA levels reaching up to 35 fold numbers in the control siRNA group compared to the others. These findings were also strongly significant in Student's t-test (p-value < 0.01). For Waga the story remains similar, except for T-antigen siRNA, which did not have an mRNA knockdown effect. For the sT and NCAN siRNAs, the Student's t-test gives significant p-values of 0.002 and 0.004 respectively for the NCAN expression levels, and 0.008 and 0.025 respectively for the LT3 expression levels. While the reduction in NCAN and LT3 expression levels is significant, we can observe that the transfection has worked better in the MKL1 cell line. This was a bit surprising, as MKL1 was one of the harder cell lines to transfect with the siGLO siRNA. However, the sample size here is small, and although these results were replicable with another reference gene (PTPRG), the

study should be replicated to verify the results and to eliminate the possibility of false positive findings.

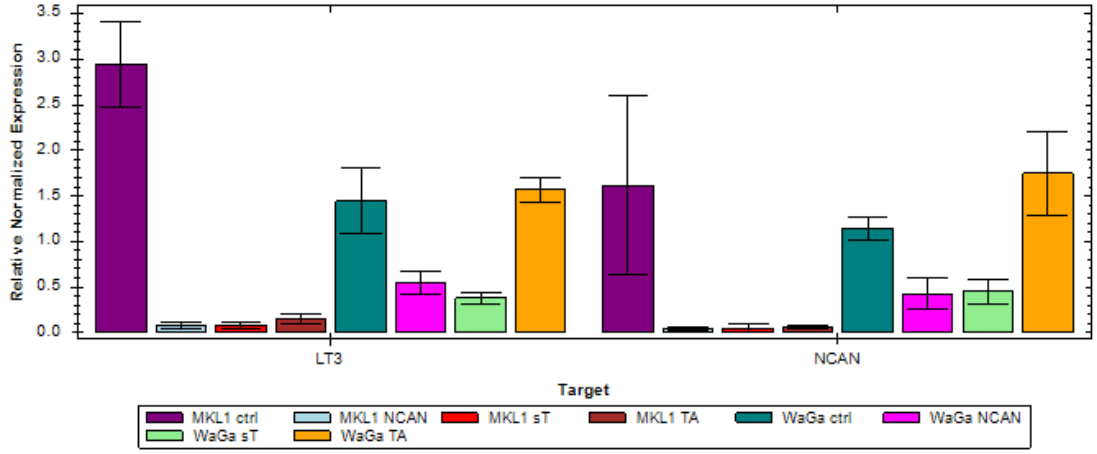

Figure 28. NCAN and LT3 mRNA expression levels after siRNA treatments in MCPyV positive cell lines. ctrl = control siRNA, NCAN = NCAN targeting siRNA, sT = small T-antigen targeting siRNA and TA = T-antigen targeting siRNA. Error bars are two times standard error of mean (2x SEM).

For the MCPyV negative cell lines the story is completely different. Neither of the cell lines tested provided any significant results, and the results resemble mostly normal biological variance in cell growth. Neither of the cell lines showed any activity in the LT3 qPCR, which was expected. In the NCAN qPCR, we can see that something went wrong with the sT siRNA treated cell lines, as the relative normalized expression in the MCC26 cell line is over 50 times higher than in any of the other siRNA treatments. While primer dimer was not the issue in this case (as proved by melting curve analysis), the problem seems to be qPCR related. The problem seems to be related to the housekeeping gene, as the average GAPDH cycle threshold value in the sT samples is much higher than in other samples. However, as this is still under investigation, we excluded the sT siRNA in the MCC negative cell lines in the qPCR, and moved on with the rest.

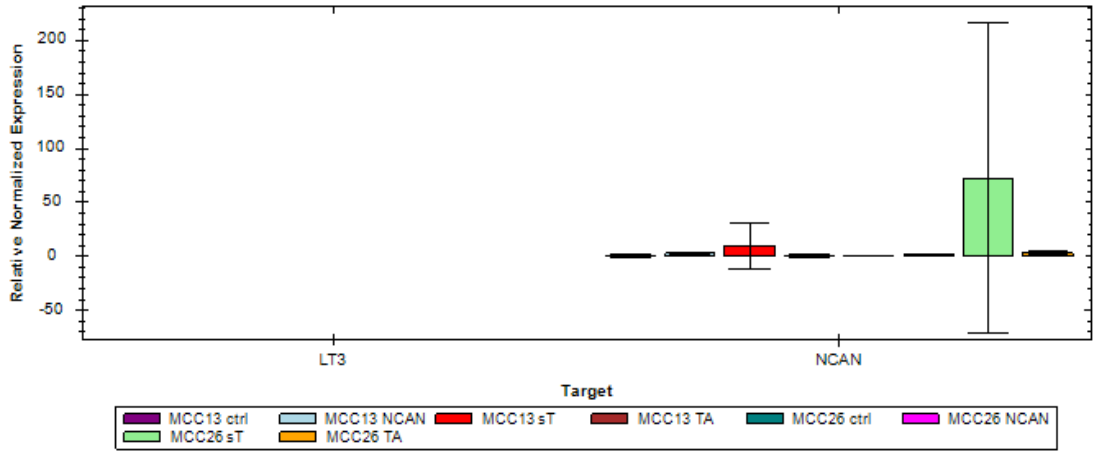

Figure 29. NCAN and LT3 mRNA expression levels after siRNA treatments in MCPyV negative cell lines. ctrl = control siRNA, NCAN = NCAN targeting siRNA, sT = small T-antigen targeting siRNA and TA = T-antigen targeting siRNA. Error bars are two times standard error of mean (2x SEM).

After the exclusion of sT, we see that the knockdown has not provided us with the expected results (Figure 30). For both of the cell lines, the non-targeting control siRNA has lower values than the targeting siRNAs. None of these findings were statistically significant, (Student's t-test, p-value > 0.5 for both cell lines and all of the targeting siRNAs.) which leads us to believe that this is a matter of biological variance in cell growth instead of a siRNA related effect. The mRNA levels of NCAN in both of the cell lines are relatively low (as visualized by Figure 25), so it is possible that neither of these cell lines actually have significant amounts of mRNA in production. These experiments should be repeated to avoid false negative results, however, as they are, they would support our hypothesis of a connection between MCPyV and NCAN.

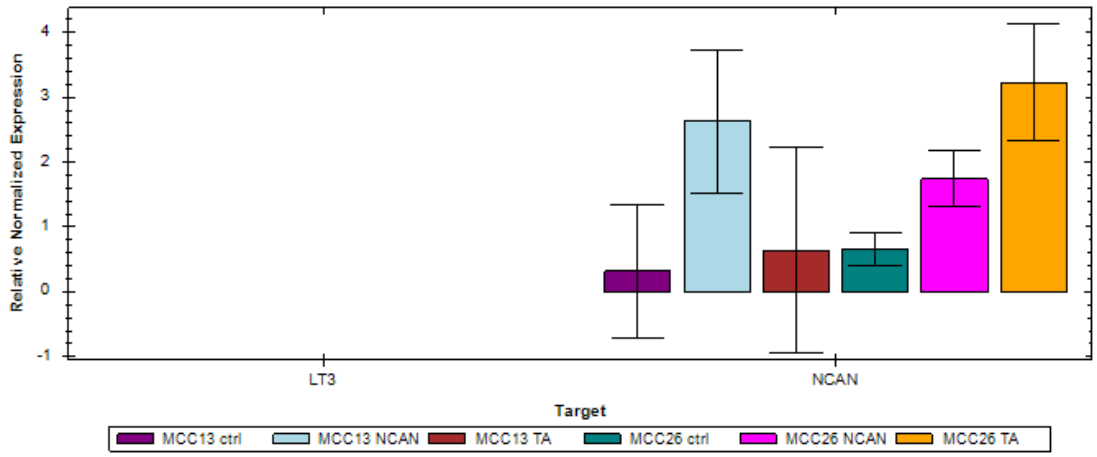

Figure 30. qPCR results in MCPyV negative cell lines after censoring sT siRNA treated groups. Error bars two times standard error of mean.

At protein level, the findings are rather disappointing. As previously described neither of the NCAN antibodies showed specific binding for the whole NCAN protein in western blots. However, as NCAN protein is highly modifiable, and like Zhang et al. showed even the cleaved versions of CSPGs can have a major effect in tumor infiltration (Zhang, Kelly et al. 1998), we proceeded to study the protein levels of siRNA knockdown models with both available antibodies. For the CM2B4 (MCPyV T-antigen) antibody, we tested only the MCPyV positive cell lines, as the MCPyV negative cell lines did not show any expression at the mRNA level, as expected.

The CM2B4 antibody did not reveal any changes in the cell lines after the siRNA treatments. Both MKL1 and WaGa cell lines had bands visible in similar sizes, but no differences could be visually detected (Figure 31). The results are similar for both of the NCAN antibodies, with a small exception in the rat specific NCAN antibody (Sigma Ald.), which showed decreased NCAN expression in the T-antigen siRNA treated WaGa cell line (Figure 32). However, this band was located at a size of roughly 70kDa, which does not represent any of the known fragment sizes of even cleaved NCAN protein. It is likely, that these bands are unspecific binding to IgG heavy chains, or some other high protein binding affinity antigen. The human specific NCAN antibody (Atlas Ab.) did not reveal any differences in the protein expression levels for either of the cell lines (Figure 33).

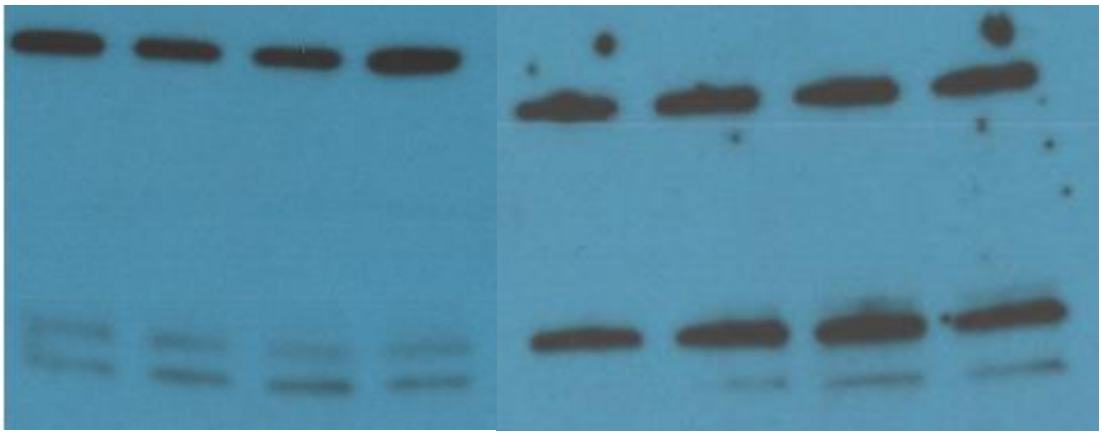

Figure 31. CM2B4 (MCPyV) antibody western blot with WaGa (left) and MKL1 (right) cell lines. The bands from left to right: control siRNA, T-antigen siRNA, sT-antigen siRNA and NCAN siRNA treated cell lines.

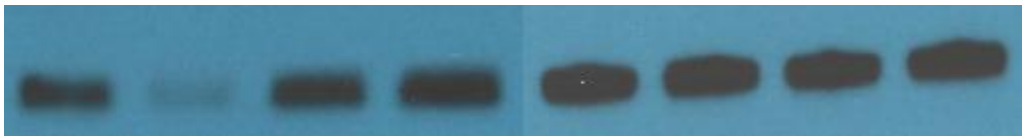

Figure 32. NCAN (Sigma Ald.) antibody western blot. WaGa (left) and MKL1 (right) cell lines, with (from left to right) control siRNA, T-antigen siRNA, sT-antigen siRNA and NCAN siRNA treatment.

Figure 33. NCAN (Atlas Ab.) antibody western blot. WaGa (left, 4 lanes) and MKL1 (right, 4 lanes) cell lines, with (from left to right) control siRNA, T-antigen siRNA, sT-antigen siRNA and NCAN siRNA treatment.

The results were highly similar for the MCPyV negative cell lines. Neither of the tested antibodies revealed any differences between the treatments (Figures 34 and 35). With the human NCAN antibody, the bands took a while longer exposure to be visible when compared to the MCPyV positive cell lines, which could indicate a difference in the protein levels between the MCPyV subgroups. However, the bands were visible and same size with the MCPyV positive cell lines, which supports the hypothesis that this is unspecific binding. While the protein expression results were underwhelming, there are a few reasons why this happened, and these will be covered in the discussion section.

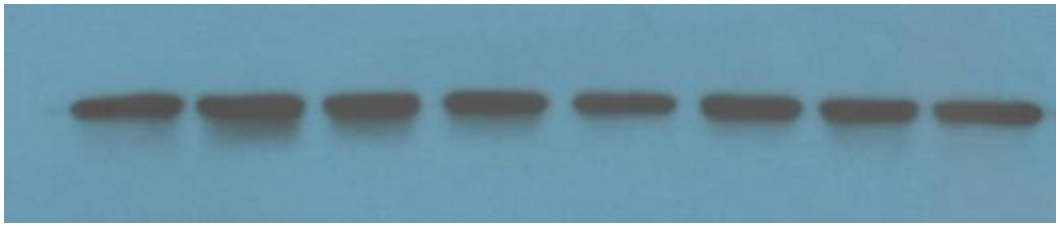

Figure 34. Figure 35. NCAN (Sigma Ald.) antibody western blot. MCC13 (left) and MCC26 (right) cell lines, with (from left to right) control siRNA, T-antigen siRNA, sT-antigen siRNA and NCAN siRNA treatment.

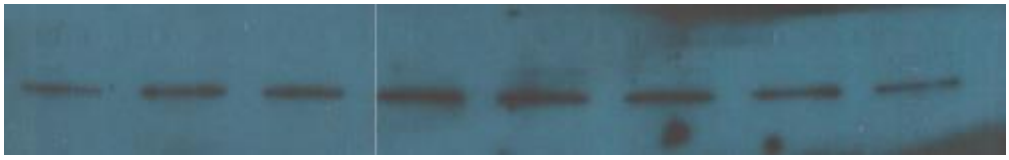

Figure 36. NCAN (Atlas Ab.) antibody western blot. MCC13 (left, 4 lanes) and MCC26 (right, 4 lanes) cell lines, with (from left to right) control siRNA, T-antigen siRNA, sT-antigen siRNA and NCAN siRNA treatment.

Cell proliferation after siRNA knockdown

For the cell proliferation assays, we used CellTiter-GLO kit (Promega) as described previously. For MKL1 we can see a small growth difference between the control siRNA treated and sT and NCAN siRNA treated goups at the 48h time point. At the 72h time point, all of the siRNA treated groups show a small growth reduction (average 8%) compared to the control group. For Waga, only sT siRNA treated group shows any reduction in growth, with 6,2% difference at 48h time point and 18% growth reduction at the 72h time point. These differences are admittedly small, and only the sT siRNA treatment of WaGa shows statistical significance (Student's t-test, p-value = 0.01). These studies were repeated twice with similar results, indicating the validity of this test. Compared to the mRNA level reduction in qPCR, these findings are underwhelming. Figure 37 visualizes these findings.

These findings are also surprising, considering that the siRNAs were designed by Kwun et al., who managed to present significant reduction in the MCPyVs viral replication and T-antigen production abilities after siRNA transfection with a similar setup to ours (Kwun, Guastafierro et al. 2009). This should lead to a significant reduction of cell growth in MCPyV positive cell lines, provided that MCPyV T-antigens have been proven to be major contributors in MCPyV dependent carcinogenesis.

The cell proliferation changes in MCPyV negative cell lines following the siRNA treatments could not be tested during the timeframe of this thesis. While the experiments were already scheduled, the recent outbreak of the COVID-19 pandemic caused significant changes in the planned experiments. However, preliminary data from the MCPyV negative MCC 26 cell line is available, as this was used in optimizing the workflow of the CellTiter-GLO assay. The cell line showed no significant changes (if any) in its growth following the siRNA treatments at 48h time point (Figure 38). This was expected, and could potentially be used (if expanded) in the future to further validate these findings.

Figure 37. Cell proliferation assay results. x-axis = 0h, 48h or 72h time point, y-axis = Luminescence counts/0,5s (Hidex Sense). . ctrl = control siRNA, NCAN = NCAN targeting siRNA, sT = small T-antigen targeting siRNA and TA = T-antigen targeting siRNA.

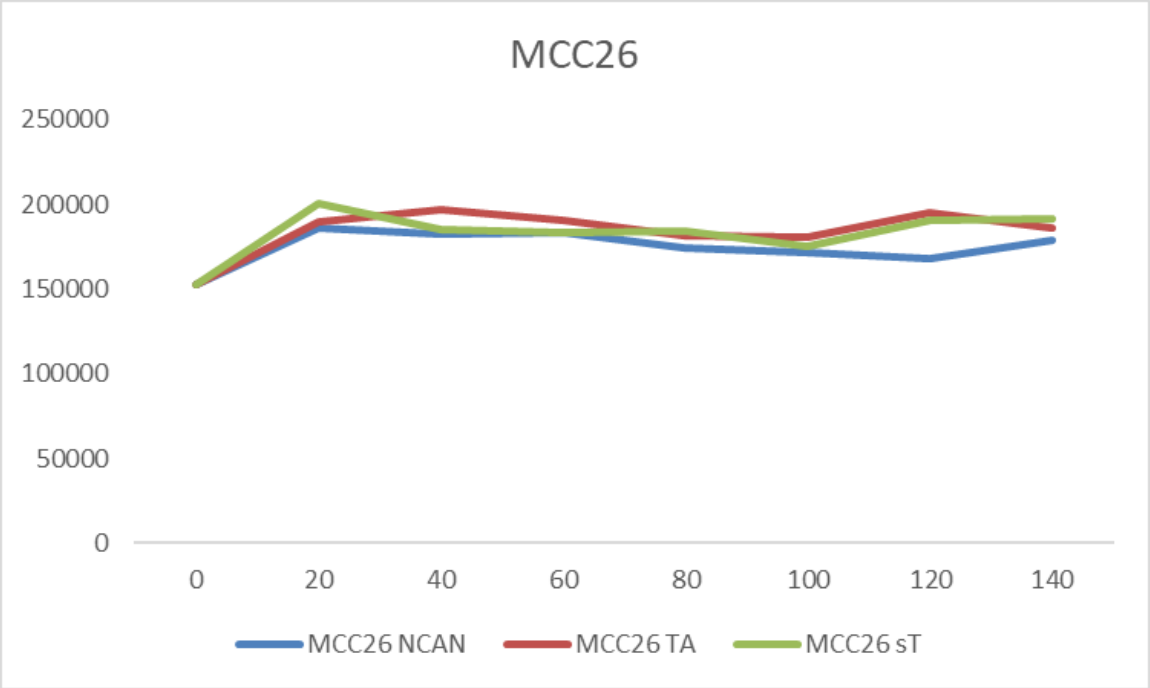

Figure 38. siRNA optimization for CellTiter-GLO with MCC26 cell line. 48h time point, x-axis siRNA concentration (nM), y-axis = Luminescence counts/0,5s (Hidex Sense)

Discussion

It is quite obvious from Figure 10 and Table 2, that the bioinformatics would have benefitted from additional gene outlier detection methods to allow for identification of common outliers across various methods. At the time of NCAN identification, no additional outlier gene detection methods were available unfortunately. This method of narrowing down the findings by inclusion of different outlier gene detection methods proved to be useful however, and the amount of data still remaining is vast. By inclusion of methods such as COPA (cancer outlier profile analysis) and outlier sum (OS) statistics could potentially reduce the number of false positive findings by “inclusion in all datasets” type of approach. As Mpindi et al. showed in their article, GTI, COPA and OS only partially overlap in outlier genes detected (Mpindi, Sara et al. 2011), which they deduced means that some or all of them must include either false positive or negative findings.

However, these methods have been commonly used in studies such as the parent project of this thesis. Thus, the research groups idea was to use novel methods to produce novel findings. This has been shown to be an effective strategy in the past by the research group members. For example, discovery of Anagrelide as a potential therapeutic drug for gastrointestinal stromal tumors was based on identification of PDE3A as an outlier gene by similar methods as ours (Pulkka, Gebreyohannes et al. 2019). And while the findings represented in this thesis might not be leading to therapeutic drug development, they still have potential as novel biomarker for MCC and could be used in the future to expand the knowledge of T-antigen functionality in MCC.

The immunohistochemistry provided us with a clear association between patients' prognosis and NCAN protein expression levels. This is in line with other studies regarding CSPGs and cancer (Zhang, Kelly et al. 1998). Our results were achievable with an untrained person (namely the author) analyzing the TMA slides while being blinded of the patients' clinical and biological data. As such, this could be easily incorporated into the clinical setting, and used by doctors when evaluating the treatments and prognosis of the patients. Complementing the IHC staining with machine learning algorithms could also potentially minimize the human errors, and produce more reliable data.

Certain aspects of the IHC staining were not described in this thesis. While NCAN is an extracellular protein and mainly secreted out of the cells, we noted that some samples included intracellular staining of the NCAN protein. This was visible throughout the different expression levels. This was studied briefly, but it had no statistical significance in patient prognosis, nor did it have any correlation with other clinical data available. And while the data gathered would suggest that MCC cell lines could technically produce NCAN protein, the source of the NCAN protein in patient samples remains unverified.

A clear downside of this study has been the small sample size. While the number of patients is extremely high considering the rarity of the cancer and the population it is derived from, it is still hard to produce reliable data from it. Firstly, since the patient samples have been collected between 1983 and 2012, a lot of variation is introduced just by time and age of the samples themselves. While it was not mentioned previously, we analyzed and discovered that the collection time of these samples did not correlate with the NCAN expression levels. When studying protein levels from FFPE samples, this is not always the case. Another problem is the scarcity of the data. For example, standard biological markers, such as cell proliferation marker Ki-67, have been studied from only a proportion of the samples available. This translates into the fact, that only 86 out of 144 samples with NCAN staining data available have also Ki-67 data available. Even obvious cases like RB and p53 had to be left out because of the low number of cases having both of the expression levels available. In the future, the dataset needs to be updated, to be able to analyze associations between these known biological markers with novel markers, such as NCAN.

The protein expression studies otherwise were a complete failure. Both the T-antigen and NCAN expression levels were uninterpretable from the western blots, the primary method for protein level expression studies planned for this project. While the T-antigen antibody was previously known to be difficult to interpret, other studies have successfully used it to interpret MCPyV T-antigen expression levels (Dye, Welcker et al. 2019). Thus, it surprised us how messy the western blots truly were. In an unpublished study, we tested these unspecific bands of the western blotting with peptide sequencing and found that the CM2B4 antibody has a high affinity towards different PP2A subunits, which is not surprising considering the interactions of T-antigens with PP2A previously described. A short literature review made it clear, that the biggest and most known research groups studying MCC are producing their antibodies by themselves. While there are clear instructions available for this sort of antibody production, the pipeline should have been built from scrap in our case, and this would have meant a lot of time spent

outside of the actual thesis. This is something to look forward to in the future, as better methods of T-antigen protein level analysis are clearly required.

When it comes to the protein levels of NCAN in MCC samples, a clear mistake was made in the designing phase of the study. Since NCAN is mainly an extracellular protein, and thus mainly excreted out of the cells, it would have made more sense to study the supernatants left from the cells instead of the cells themselves. Methods such as ELISA could have easily been incorporated into the study, had this occurred to us at an earlier phase. However, the COVID-19 pandemic prevented us from doing such measures (not to speak of preventing us from replicating our results). With the limited timeframe of a masters' thesis, this is the best we could come up with. However, the secreted NCAN levels will be studied in the future, as the situation with COVID-19 gets easier.

For the qPCR, everything seemed to work as intended. The primers were tested beforehand (data not shown), and they produced a product of the predicted size in standard PCR. While originally designed for Roche Universal ProbeLibrary qPCR assay, the primers were suited for other qPCR assays and even surpassed the Roches method. Biological replicates were not introduced to the experiments, solely due to time constraints. This does have an impact on the reliability of the results and will be attended to afterwards.

While we were happy with the transfection efficacy after the optimization periods, it is to be said that much more could have been done here. First of all, the results from T-antigen knockdown are a mixed bag. The mRNA levels of all of MKL1 cell line with all of the different siRNA treatments are significantly lower than those of the control groups. This was also the case in NCAN and sT siRNA treated WaGa cells, where as neither of the MCPyV negative cell lines responded to either treatment. This would indicate a successful transfection. While this could not be verified on the protein level, due to improper detection methods used and poor antibodies, the initial response was positive.

However, in case of proper siRNA transfection efficiency and T-antigen siRNA targeting, we would assume to reach significant growth reduction of the MCPyV positive cell lines. This has been the case for a number of studies including those of Houben et al. and Shuda et al. (Houben, Shuda et al. 2010, Shuda, Kwun et al. 2011). However, many have used shRNAs and viral transfection instead of siRNA combined with transfection reagent such as lipofectamine. This and the fact that sT siRNA treated WaGa cell line and all of the treated MKL1 cell lines showed slight growth reduction (sT WaGa being the only statistically significant one) would indicate that the transfection efficiency was our downfall in this study. There are a vast amount of different transfection reagents available, as well as completely different silencing methods (like the before mentioned shRNAs and CRISPR technologies to name a few), so achieving better transfection efficiencies and thus better gene knockdown effects is only a matter of optimization.

However, the slight growth reduction that we achieved does raise more questions, which is often a positive outcome of an experiment. For example, while the transfection worked based on the mRNA levels, why did it not transfer into the cell proliferation level? One possibility is yet again in the methods used. Due to

the MCPyV positive cells growing in suspension, we could not change the growth media of the cells prior to administration of the siRNAs. There is a possibility that the cells have secreted a sufficient amount of T-antigens and NCAN into the growth medium, delaying the impact of a siRNA transfection. This could be indicated by the late response to the T-antigen siRNA treatment in MKL1 cells, as seen in Figure 37. However, in the case of T-antigen this has not been reported, and it seems unlikely, as T-antigens are used mainly intracellularly. Another option is that the amount of NCAN and T-antigen produced are so low, that the qPCR results give falsely high expression level changes as a result. As mentioned previously, other groups have successfully transfected MCC cell lines with T-antigen targeting siRNAs and shown significant growth reduction, so this is unlikely.

The role of NCAN in MCC remains elusive. The patient data shows that low NCAN expression associates to worse patient prognosis. This combined with the findings of Zhang et al. and Silver et al. supports a hypothesis (Silver et al.) that NCAN (like other CSPGs) would have an inhibitory role in tumor invasiveness more than an invasion promoting effect (Zhang, Kelly et al. 1998, Silver, D. J., Siebzehnrubl et al. 2013, Silver, D. J., Silver 2014). However, looking at the qPCR data, we see that targeting NCAN with siRNAs decreases the LT3 expression and vice versa, suggesting a possible signaling loop between these two proteins. This needs to be further investigated, as it could provide important insight into the tumor microenvironment and tumor invasion properties of MCPyV positive MCCs.

Conclusions

Overall, the primary results of this thesis were partially satisfied. We identified a novel biomarker specific for the MCPyV positive subtype of Merkel cell carcinoma based on bioinformatics data, and proved that the specificity carries over to our patient data as well as MCC cell lines in our collection. Low NCAN expression was significantly associated to poor patient prognosis in immunohistochemistry, however, Cox proportional hazards model revealed that NCAN is not an independent variable in patient survival. Other clinical factors, such as patient age and gender, did not associate significantly with NCAN expression levels.

Low NCAN expression is associated with MCPyV negative subtype in MCC cell lines at mRNA level. The protein levels remain inconclusive, due to mistakes in experimental design and poor antibody specificity in western blotting. This result further indicates that there is a significant difference in NCAN expression in different MCC subtypes.

siRNA knockdown of NCAN reduced the expression of both NCAN and LT3 (MCPyV T-antigen) significantly in MCPyV positive cell lines at mRNA levels. Similarly, the knockdown of both small T-antigen and the large (complete) T-antigen reduced the expression of NCAN in MCPyV positive cell lines in qPCR. Complementary, the MCPyV negative cell lines saw no significant changes, with any siRNA treatments when compared to the control treatment. This suggests there might be a signaling loop of sorts between the MCPyV T-antigens and NCAN.

All of the siRNA treatments on MKL1 cell line had a slight but not significant reduction in their growth. Only sT siRNA treated WaGa cells showed any response to the treatment, however, this was statistically significant finding. MCPyV negative cell lines were not properly tested due to time shortage caused by the recent outbreak of COVID-19 pandemic. Other functional studies that had been planned, such as cell migration and invasion assays, were also cancelled due to lack of time.

Acknowledgements

I would like to thank the entire Rare Cancers Research group for giving me the opportunity to study NCAN as described in this thesis. I would also like to give special thanks to:

Harri Sihto for trusting this project on my hands and supervising what could be described only as struggles that I had with/during this project.

Nanna Merikoski for helping me not only with my hands on work, but also with my mental stability during my master's thesis project.

References

AMERICAN CANCER SOCIETY, 2019-last update, Merkel Cell Carcinoma Stages. Available: https://www.cancer.org/cancer/merkel-cell-skin-cancer/detection-diagnosis-staging/staging.html [Apr 23, 2020].

AVDULOV, S., LI, S., VAN MICHALEK, BURRICHTER, D., PETERSON, M., PERLMAN, D.M., MANIVEL, J.C., SONENBERG, N., YEE, D., BITTERMAN, P.B. and POLUNOVSKY, V.A., 2004. *Activation of translation complex eIF4F is essential for the genesis and maintenance of the malignant phenotype in human mammary epithelial cells.*

BECKER, J.C., SCHRAMA, D. and HOUBEN, R., 2008. Merkel cell carcinoma. *Cellular and Molecular Life Sciences,* **66**(1), pp. 1.

BHATIA, S., STORER, B.E., IYER, J.G., MOSHIRI, A., PARVATHANENI, U., BYRD, D., SOBER, A.J., SONDAK, V.K., GERSHENWALD, J.E. and NGHIEM, P., 2016. Adjuvant Radiation Therapy and Chemotherapy in Merkel Cell Carcinoma: Survival Analyses of 6908 Cases From the National Cancer Data Base. *JNCI: Journal of the National Cancer Institute,* **108**(9), pp. djw042.

BORCHERT, S., CZECH-SIOLI, M., NEUMANN, F., SCHMIDT, C., WIMMER, P., DOBNER, T., GRUNDHOFF, A. and FISCHER, N., 2014. High-affinity Rb binding, p53 inhibition, subcellular localization, and transformation by wild-type or tumor-derived shortened Merkel cell polyomavirus large T antigens. *Journal of virology,* **88**(6), pp. 3144-3160.

BOYAPATI, A., WILSON, M., YU, J. and RUNDELL, K., 2003. *SV40 17KT antigen complements dnaj mutations in large T antigen to restore transformation of primary human fibroblasts.*

CALVIGNAC-SPENCER, S., FELTKAMP, M.C.W., DAUGHERTY, M.D., MOENS, U., RAMQVIST, T., JOHNE, R., EHLERS, B. and POLYOMAVIRIDAE STUDY GROUP OF THE INTERNATIONAL COMMITTEE ON TAXONOMY, OF VIRUSES, 2016. A taxonomy update for the family Polyomaviridae. *Archives of Virology,* **161**(6), pp. 1739-1750.

CHANG, Y., CESARMAN, E., PESSIN, M.S., LEE, F., CULPEPPER, J., KNOWLES, D.M. and MOORE, P.S., 1994. Identification of herpesvirus-like DNA sequences in AIDS-associated Kaposi's sarcoma. *Science,* **266**(5192), pp. 1865-1869.

CORLEY, S.M., TROY, N.M., BOSCO, A. and WILKINS, M.R., 2019. QuantSeq. 3′ Sequencing combined with Salmon provides a fast, reliable approach for high throughput RNA expression analysis. *Scientific Reports,* **9**(1), pp. 18895.

DYE, K.N., WELCKER, M., CLURMAN, B.E., ROMAN, A. and GALLOWAY, D.A., 2019. Merkel cell polyomavirus Tumor antigens expressed in Merkel cell

carcinoma function independently of the ubiquitin ligases Fbw7 and β-TrCP. *PLoS pathogens,* **15**(1), pp. e1007543.

ENGELS, E.A., FRISCH, M., GOEDERT, J.J., BIGGAR, R.J. and MILLER, R.W., 2002. *Merkel cell carcinoma and HIV infection.*

FANHCHAKSAI, K., OKADA, F., NAGAI, N., POTHACHAROEN, P., KONGTAWELERT, P., HATANO, S., MAKINO, S., NAKAMURA, T. and WATANABE, H., 2016. Host stromal versican is essential for cancer-associated fibroblast function to inhibit cancer growth. *International Journal of Cancer,* **138**(3), pp. 630-641.

FEMIA, D., PRINZI, N., ANICHINI, A., MORTARINI, R., NICHETTI, F., CORTI, F., TORCHIO, M., PEVERELLI, G., PAGANI, F., MAURICHI, A., MATTAVELLI, I., MILIONE, M., BEDINI, N., CORTI, A., DI BARTOLOMEO, M., DE BRAUD, F. and PUSCEDDU, S., 2018. Treatment of Advanced Merkel Cell Carcinoma: Current Therapeutic Options and Novel Immunotherapy Approaches. *Targeted Oncology,* **13**(5), pp. 567-582.

FENG, H., KWUN, H.J., LIU, X., GJOERUP, O., STOLZ, D.B., CHANG, Y. and MOORE, P.S., 2011. Cellular and viral factors regulating Merkel cell polyomavirus replication. *PloS one,* **6**(7), pp. e22468.

FENG, H., SHUDA, M., CHANG, Y. and MOORE, P.S., 2008. Clonal Integration of a Polyomavirus in Human Merkel Cell Carcinoma. *Science,* **319**(5866), pp. 1096-1100.

FRISCHKNECHT, R. and SEIDENBECHER, C.I., 2008. The crosstalk of hyaluronan-based extracellular matrix and synapses. *Neuron Glia Biology,* **4**(3), pp. 249-257.

GARNESKI, K.M. and NGHIEM, P., 2007. *Merkel cell carcinoma adjuvant therapy: Current data support radiation but not chemotherapy.*

GIRSCHIK, J., THORN, K., BEER, T.W., HEENAN, P.J. and FRITSCHI, L., 2011. Merkel cell carcinoma in Western Australia: a population-based study of incidence and survival. *British Journal of Dermatology,* **165**(5), pp. 1051-1057.

GOOPTU, C., WOOLLONS, A., ROSS, J., PRICE, M., WOJNAROWSKA, F., MORRIS, P.J., WALL, S. and BUNKER, C.B., 1997. Merkel cell carcinoma arising after therapeutic immunosuppression. *British Journal of Dermatology,* **137**(4), pp. 637-641.

GRIM, M. and HALATA, Z., 2000. Developmental origin of avian Merkel cells. *Anatomy and Embryology,* **202**(5), pp. 401-410.

GRIMPE, B., PRESSMAN, Y., BUNGE, M.B. and SILVER, J., 2005. *The role of proteoglycans in Schwann cell/astrocyte interactions and in regeneration failure at PNS/CNS interfaces.*

HARMS, P.W., HARMS, K.L., MOORE, P.S., DECAPRIO, J.A., NGHIEM, P., WONG, M.K.K., BROWNELL, I. and ON BEHALF OF THE INTERNATIONAL WORKSHOP ON MERKEL CELL CARCINOMA RESEARCH (IWMCC), WORKING GROUP, 2018. The biology and treatment of Merkel cell carcinoma: current understanding and research priorities. *Nature Reviews Clinical Oncology,* **15**(12), pp. 763-776.

HARMS, P.W., VATS, P., VERHAEGEN, M.E., ROBINSON, D.R., WU, Y., DHANASEKARAN, S.M., PALANISAMY, N., SIDDIQUI, J., CAO, X., SU, F., WANG, R., XIAO, H., KUNJU, L.P., MEHRA, R., TOMLINS, S.A., FULLEN, D.R., BICHAKJIAN, C.K., JOHNSON, T.M., DLUGOSZ, A.A. and CHINNAIYAN, A.M., 2015. The Distinctive Mutational Spectra of Polyomavirus-Negative Merkel Cell Carcinoma. *Cancer research,* **75**(18), pp. 3720-3727.

HARRINGTON, C. and KWAN, W., 2014. Outcomes of Merkel Cell Carcinoma Treated with Radiotherapy without Radical Surgical Excision. *Annals of Surgical Oncology,* **21**(11), pp. 3401-3405.

HEATH, M., JAIMES, N., LEMOS, B., MOSTAGHIMI, A., WANG, L.C., PEÑAS, P.F. and NGHIEM, P., 2008. *Clinical characteristics of Merkel cell carcinoma at diagnosis in 195 patients: the AEIOU features.*

HENKE, E., NANDIGAMA, R. and ERGÜN, S., 2020. Extracellular Matrix in the Tumor Microenvironment and Its Impact on Cancer Therapy. *Frontiers in molecular biosciences,* **6**, pp. 160.

HODGSON, N.C., 2005. Merkel cell carcinoma: Changing incidence trends. *Journal of surgical oncology,* **89**(1), pp. 1-4.

HOUBEN, R., SHUDA, M., WEINKAM, R., SCHRAMA, D., FENG, H., CHANG, Y., MOORE, P.S. and BECKER, J.C., 2010. Merkel Cell Polyomavirus-Infected Merkel Cell Carcinoma Cells Require Expression of Viral T Antigens. *Journal of virology,* **84**(14), pp. 7064-7072.

HWANG, J.H.K., ALANEN, K., DABBS, K.D., DANYLUK, J. and SILVERMAN, S., 2008. Merkel cell carcinoma with squamous and sarcomatous differentiation. *Journal of cutaneous pathology,* **35**(10), pp. 955-959.

JOHNE, R., BUCK, C.B., ALLANDER, T., ATWOOD, W.J., GARCEA, R.L., IMPERIALE, M.J., MAJOR, E.O., RAMQVIST, T. and NORKIN, L.C., 2011. Taxonomical developments in the family Polyomaviridae. *Archives of Virology,* **156**(9), pp. 1627-1634.

KHALILI, K., SARIYER, I.K. and SAFAK, M., 2008. Small tumor antigen of polyomaviruses: Role in viral life cycle and cell transformation. *Journal of cellular physiology,* **215**(2), pp. 309-319.

KOLJONEN, V., 2006. Merkel cell carcinoma. *World Journal of Surgical Oncology,* **4**(1), pp. 7.

KUFFLER, D.P., SOSA, I.J. and REYES, O., 2009. Schwann cell chondroitin sulfate proteoglycan inhibits dorsal root ganglion neuron neurite outgrowth and substrate specificity via a soma and not a growth cone mechanism. *Journal of neuroscience research,* **87**(13), pp. 2863-2871.

KUKKO, H., BÖHLING, T., KOLJONEN, V., TUKIAINEN, E., HAGLUND, C., POKHREL, A., SANKILA, R. and PUKKALA, E., 2012. *Merkel cell carcinoma – A population-based epidemiological study in Finland with a clinical series of 181 cases.*

KWUN, H.J., GUASTAFIERRO, A., SHUDA, M., MEINKE, G., BOHM, A., MOORE, P.S. and CHANG, Y., 2009. The Minimum Replication Origin of Merkel Cell Polyomavirus Has a Unique Large T-Antigen Loading Architecture and Requires Small T-Antigen Expression for Optimal Replication. *Journal of virology,* **83**(23), pp. 12118-12128.

LAU, L.W., CUA, R., KEOUGH, M.B., HAYLOCK-JACOBS, S. and YONG, V.W., 2013. Pathophysiology of the brain extracellular matrix: a new target for remyelination. *Nature Reviews Neuroscience,* **14**, pp. 722.

LEMOS, B.D., STORER, B.E., IYER, J.G., PHILLIPS, J.L., BICHAKJIAN, C.K., FANG, L.C., JOHNSON, T.M., LIEGEOIS-KWON, N.J., OTLEY, C.C., PAULSON, K.G., ROSS, M.I., YU, S.S., ZEITOUNI, N.C., BYRD, D.R., SONDAK, V.K., GERSHENWALD, J.E., SOBER, A.J. and NGHIEM, P., 2010. *Pathologic nodal evaluation improves prognostic accuracy in Merkel cell carcinoma: Analysis of 5823 cases as the basis of the first consensus staging system.*

LEXOGEN, 2019-last update, QuantSeq 3' mRNA Sequencing Workflow. Available: https://www.lexogen.com/quantseq-workflow/ [Mar 12, 2020].

MCRAE, P.A. and PORTER, B.E., 2012. *The perineuronal net component of the extracellular matrix in plasticity and epilepsy.*

MEDISAPIENS LTD., 2019. *MediSapiens report 23.04.2019.*

MEDISAPIENS LTD., 2011-last update, IST online database. Available: https://ist.medisapiens.com/ [23.04., 2020].

MILLER, N.J., CHURCH, C.D., FLING, S.P., KULIKAUSKAS, R., RAMCHURREN, N., SHINOHARA, M.M., KLUGER, H.M., BHATIA, S., LUNDGREN, L., CHEEVER, M.A., TOPALIAN, S.L. and NGHIEM, P., 2018. Merkel cell polyomavirus-specific immune responses in patients with Merkel cell carcinoma receiving anti-PD-1 therapy. *Journal for immunotherapy of cancer,* **6**(1), pp. 131.

MOGHA, A., FAUTREL, A., MOUCHET, N., GUO, N., CORRE, S., ADAMSKI, H., WATIER, E., MISERY, L. and GALIBERT, M., 2010. Merkel cell polyomavirus small T antigen mRNA level is increased following in vivo UV-radiation. *PloS one,* **5**(7), pp. e11423.

MORRIS, L.G.T., TAYLOR, B.S., BIVONA, T.G., GONG, Y., ENG, S., BRENNAN, C.W., KAUFMAN, A., KASTENHUBER, E.R., BANUCHI, V.E., SINGH, B., HEGUY, A., VIALE, A., MELLINGHOFF, I.K., HUSE, J., GANLY, I. and CHAN, T.A., 2011. Genomic dissection of the epidermal growth factor receptor (EGFR)/PI3K pathway reveals frequent deletion of the EGFR phosphatase PTPRS in head and neck cancers. *Proceedings of the National Academy of Sciences of the United States of America,* **108**(47), pp. 19024-19029.

MPINDI, J.P., SARA, H., HAAPA-PAANANEN, S., KILPINEN, S., PISTO, T., BUCHER, E., OJALA, K., ILJIN, K., VAINIO, P., BJÖRKMAN, M., GUPTA, S., KOHONEN, P., NEES, M. and KALLIONIEMI, O., 2011. GTI: A Novel Algorithm for Identifying Outlier Gene Expression Profiles from Integrated Microarray Datasets. *PLOS ONE,* **6**(2), pp. e17259.

NISCHALKE, H.D., LUTZ, P., KRÄMER, B., SÖHNE, J., MÜLLER, T., ROSENDAHL, J., FISCHER, J., BERG, T., HITTATIYA, K., FISCHER, H., SOYKA, M., SEMMO, N., NATTERMANN, J., SAUERBRUCH, T., STRASSBURG, C.P., STICKEL, F. and SPENGLER, U., 2014. *A common polymorphism in the NCAN gene is associated with hepatocellular carcinoma in alcoholic liver disease.*

PRANGE, C.K., PENNACCHIO, L.A., LIEUALLEN, K., FAN, W. and LENNON, G.G., 1998. *Characterization of the human neurocan gene, CSPG31The nucleotide sequence reported in this paper has been submitted to the GenBank Database under the name CSPG3 and accession number AF026547.1.*

PULKKA, O., GEBREYOHANNES, Y.K., WOZNIAK, A., MPINDI, J., TYNNINEN, O., ICAY, K., CERVERA, A., KESKITALO, S., MURUMÄGI, A., KULESSKIY, E., LAAKSONEN, M., WENNERBERG, K., VARJOSALO, M., LAAKKONEN, P., LEHTONEN, R., HAUTANIEMI, S., KALLIONIEMI, O., SCHÖFFSKI, P., SIHTO, H. and JOENSUU, H., 2019. Anagrelide for Gastrointestinal Stromal Tumor. *Clinical Cancer Research,* **25**(5), pp. 1676-1687.

RAUCH, U., GRIMPE, B., KULBE, G., ARNOLD-AMMER, I., BEIER, D.R. and FÄSSLER, R.F., 1995. *Structure and Chromosomal Localization of the Mouse Neurocan Gene.*

SHEN, Y., TENNEY, A.P., BUSCH, S.A., HORN, K.P., CUASCUT, F.X., LIU, K., HE, Z., SILVER, J. and FLANAGAN, J.G., 2009. PTPsigma is a receptor for chondroitin sulfate proteoglycan, an inhibitor of neural regeneration. *Science (New York, N.Y.),* **326**(5952), pp. 592-596.

SHERR, C.J., 2000. The Pezcoller Lecture: Cancer Cell Cycles Revisited. *Cancer research,* **60**(14), pp. 3689-3695.

SHUDA, M., FENG, H., KWUN, H.J., ROSEN, S.T., GJOERUP, O., MOORE, P.S. and CHANG, Y., 2008. T antigen mutations are a human tumor-specific signature for Merkel cell polyomavirus. *Proceedings of the National Academy of Sciences,* **105**(42), pp. 16272-16277.

SHUDA, M., KWUN, H.J., FENG, H., CHANG, Y. and MOORE, P.S., 2011. Human Merkel cell polyomavirus small T antigen is an oncoprotein targeting the 4E-BP1 translation regulator. *The Journal of clinical investigation,* **121**(9), pp. 3623-3634.

SIHTO, H., KUKKO, H., KOLJONEN, V., SANKILA, R., BÖHLING, T. and JOENSUU, H., 2011. Merkel Cell Polyomavirus Infection, Large T Antigen, Retinoblastoma Protein and Outcome in Merkel Cell Carcinoma. *Clinical Cancer Research,* **17**(14), pp. 4806-4813.

SIHTO, H., KUKKO, H., KOLJONEN, V., SANKILA, R., BÖHLING, T. and JOENSUU, H., 2009. Clinical Factors Associated With Merkel Cell Polyomavirus Infection in Merkel Cell Carcinoma. *JNCI: Journal of the National Cancer Institute,* **101**(13), pp. 938-945.

SILVER, D.J., SIEBZEHNRUBL, F.A., SCHILDTS, M.J., YACHNIS, A.T., SMITH, G.M., SMITH, A.A., SCHEFFLER, B., REYNOLDS, B.A., SILVER, J. and STEINDLER, D.A., 2013. Abstract 1639: Chondroitin sulfate proteoglycans potently inhibit invasion and serve as a central organizer of the brain tumor microenvironment. *Cancer research,* **73**(8 Supplement), pp. 1639.

SILVER, D.J. and SILVER, J., 2014. *Contributions of chondroitin sulfate proteoglycans to neurodevelopment, injury, and cancer.*

SILVER, J. and MILLER, J.H., 2004. Regeneration beyond the glial scar. *Nature Reviews Neuroscience,* **5**(2), pp. 146-156.

SNOW, D.M., STEINDLER, D.A. and SILVER, J., 1990. *Molecular and cellular characterization of the glial roof plate of the spinal cord and optic tectum: A possible role for a proteoglycan in the development of an axon barrier.*

STUBDAL, H., ZALVIDE, J., CAMPBELL, K.S., SCHWEITZER, C., ROBERTS, T.M. and DECAPRIO, J.A., 1997. Inactivation of pRB-related proteins p130 and p107 mediated by the J domain of simian virus 40 large T antigen. *Molecular and cellular biology,* **17**(9), pp. 4979-4990.

SU, Z., KISHIDA, S., TSUBOTA, S., SAKAMOTO, K., CAO, D., KIYONARI, S., OHIRA, M., KAMIJO, T., NARITA, A., XU, Y., TAKAHASHI, Y. and KADOMATSU, K., 2017. Neurocan, an extracellular chondroitin sulfate proteoglycan, stimulates neuroblastoma cells to promote malignant phenotypes. *Oncotarget,* **8**(63), pp. 106296-106310.

SUBRAMANIAN, A., TAMAYO, P., MOOTHA, V.K., MUKHERJEE, S., EBERT, B.L., GILLETTE, M.A., PAULOVICH, A., POMEROY, S.L., GOLUB, T.R., LANDER, E.S. and MESIROV, J.P., 2005. Gene set enrichment analysis: A knowledge-based approach for interpreting genome-wide expression profiles. *Proceedings of the National Academy of Sciences,* **102**(43), pp. 15545-15550.

SULLIVAN, C.S. and PIPAS, J.M., 2002. T antigens of simian virus 40: molecular chaperones for viral replication and tumorigenesis. *Microbiology and molecular biology reviews : MMBR,* **66**(2), pp. 179-202.

SZEDER, V., GRIM, M., HALATA, Z. and SIEBER-BLUM, M., 2003. *Neural crest origin of mammalian Merkel cells.*

TANG, C. and TOKER, C., 1978. Trabecular carcinoma of the skin. An ultrastructural study. *Cancer,* **42**(5), pp. 2311-2321.

TELLO, T.L., COGGSHALL, K., YOM, S.S. and YU, S.S., 2018. *Merkel cell carcinoma: An update and review: Current and future therapy.*

TOKER, C., 1972. Trabecular Carcinoma of the Skin. *Archives of Dermatology,* **105**(1), pp. 107-110.

TONG, P., CHEN, Y., SU, X. and COOMBES, K.R., 2013. SIBER: systematic identification of bimodally expressed genes using RNAseq data. *Bioinformatics,* **29**(5), pp. 605-613.

VARGA, I., HUTÓCZKI, G., PETRÁS, M., SCHOLTZ, B., MIKÓ, E., KENYERES, A., TÓTH, J., ZAHUCZKY, G., BOGNÁR, L., HANZÉLY, Z. and KLEKNER, A., 2010. Expression of Invasion-Related Extracellular Matrix Molecules in Human Glioblastoma Versus Intracerebral Lung Adenocarcinoma Metastasis. *Central European Neurosurgery - Zentralblatt für Neurochirurgie,* **71**(04), pp. 173-180.

VARGA, I., HUTÓCZKI, G., SZEMCSÁK, C.D., ZAHUCZKY, G., TÓTH, J., ADAMECZ, Z., KENYERES, A., BOGNÁR, L., HANZÉLY, Z. and KLEKNER, A., 2012. Brevican, Neurocan, Tenascin-C and Versican are Mainly Responsible for the Invasiveness of Low-Grade Astrocytoma. *Pathology & Oncology Research,* **18**(2), pp. 413-420.

VOOG, E., BIRON, P., MARTIN, J. and BLAY, J., 1999. Chemotherapy for patients with locally advanced or metastatic Merkel cell carcinoma. *Cancer,* **85**(12), pp. 2589-2595.

WALSH, N.M.G., 2001. *Primary neuroendocrine (Merkel cell) carcinoma of the skin: Morphologic diversity and implications thereof.*

YAO, J., TUCKER, B.A., ZHANG, X., CHECA-CASALENGUA, P., HERRERO-VANRELL, R. and YOUNG, M.J., 2011. *Robust cell integration from co-transplantation of biodegradable MMP2-PLGA microspheres with retinal progenitor cells.*

ZHANG, H., KELLY, G., ZERILLO, C., JAWORSKI, D.M. and HOCKFIELD, S., 1998. Expression of a cleaved brain-specific extracellular matrix protein mediates glioma cell invasion In vivo. *The Journal of neuroscience : the official journal of the Society for Neuroscience,* **18**(7), pp. 2370-2376.

ZUR HAUSEN, A., RENNSPIESS, D., WINNEPENNINCKX, V., SPEEL, E.M. and KURZ, A.K., 2013. Early B-cell differentiation in Merkel cell carcinomas: clues to cellular ancestry. *Cancer research,* , pp. canres.0616.2013.

Appendices

Appendix 1. Primers used in the project

Pri-mers	Gene Ensembl ID:	Amplicon length	Pri-mer	
GAPDH	ENSG00000111640	80	for	
			rev	
LT3	NA	NA	for	
			rev	
NCAN	ENSG00000130287.13	84	for	
			rev	
PTPRG	ENSG00000144724	NA	for	
			rev	
Pri-mers	Sequence 5' - 3'	TM	GC%	Position
GAPDH	TCAAGATCATCAGCAATGCC	58	45	6537204-6537315
	CGATACCAAAGTTGTCATGGA	58	43	6537356-6537376
LT3	GCATCTGCACCTTTTCTAGACTC	NA	NA	NA
	TTTTGCCTTATA-GACTTTTCCATATCT			
NCAN	GGCAGCTTTTGTGAGAAAGAC	59	48	3331 - 3351
	GTGGGCAAAATAGCGGTAAC	59	50	3395 - 3414
PTPRG	TATGGGAGTGTGGGATGGTT	NA	NA	NA
	TAAGCTGGGAGGATCGCTTA			

Appendix 2. Immunohistochemistry protocols

NCAN (Atlas AB: HPA036814) IHC
Antibody produced in Rabbit Salmikangas 2019

1. Xyl-, descending EtOH-series, H_2O wash
2. 30 min H_2O_2 (200ml H_2O + 5ml H_2O_2 35%)
3. 2 x H_2O wash
4. HIER with EnVision™ Flex Target Retrieval solution Low pH buffer, 15min 95C, let cool for 2h
5. 2 x wash with TBS
6. Dilute **NCAN 1:200** with Draco antibody diluent
   - **150ul / slide + overnight incubation +4C**
7. 2x TBS wash
8. WellMed Orion detection system, **Rabbit HRP 150uL/slide, 60min RT'**
9. 2x TBS wash
10. Dilute DAB (ImmPact DAB) **1mL buffer + 1 drop of DAB, 100uL/slide, 5min RT'**
11. 2x TBS wash
12. H_2O wash
13. Hematoxylin1 min + 10 min under running water
14. Rising EtOH-series, Xylene and covering with permount

Appendix 3. Western blot protocols

NCAN (Atlas Antibodies: HPA036814) Western blot
Antibody produced in Rabbit Salmikangas 2020

1. Pipette 5µg of each pretreated and denatured protein lysate and protein ladder on SDS-PAGE gel
2. Run the gel with **100V constant** for roughly **1,5 hours**, or until the leading buffer nears the end of the gel
3. Remove the gel from the holder and stack it in between the **Trans-Blot Turbo Transfer Pack.** The bottom and top portions are labeled, and the gel comes in between them.
4. Transfer the proteins to the PVDF membrane included in the transfer pack with Bio-Rad **Trans-Blot Turbo.** Use the pre-installed protocol **Mixed molecular weights**, 1,3A, 7min.
5. Block the membrane with **5% skimmed milk in WB Wash Buffer**
6. Wash the membrane three times with WB Wash Buffer (Optional), 5 minutes on a shaker
7. Dilute **NCAN primary antibody 1:1000** in **1% skimmed milk in WB Wash Buffer**
    a. Incubate the membrane in the primary antibody **overnight in +4°C**
8. Wash the membrane three times with WB Wash Buffer, 5 minutes on a shaker
9. Dilute **mouse-anti-Rabbit secondary antibody 1:10 000** in **1% skimmed milk in WB Wash Buffer**
    a. Incubate the membrane in the secondary antibody for **1h at room temperature**
10. Wash the membrane three times with WB Wash Buffer, 5 minutes on a shaker
11. Mix equal volumes of SuperSignal West Pico PLUS reagents, and incubate the membrane for **5 minutes at room temperature**
12. Visualize the membrane with x-ray film exposure.

WB Wash Buffer = non sterile TBS + 0,1% Tween20

NCAN (Merck/Sigma: N0913) Western blot
Antibody produced in Mouse Salmikangas 2020

1. Pipette 5µg of each pretreated and denatured protein lysate and protein ladder on SDS-PAGE gel
2. Run the gel with **100V constant** for roughly **1,5 hours**, or until the leading buffer nears the end of the gel
3. Remove the gel from the holder and stack it in between the **Trans-Blot Turbo Transfer Pack.** The bottom and top portions are labeled, and the gel comes in between them.
4. Transfer the proteins to the PVDF membrane included in the transfer pack with Bio-Rad **Trans-Blot Turbo.** Use the pre-installed protocol **Mixed molecular weights**, 1,3A, 7min.
5. Block the membrane with **5% skimmed milk in WB Wash Buffer**
6. Wash the membrane three times with WB Wash Buffer (Optional), 5 minutes on a shaker
7. Dilute **NCAN primary antibody 1:1000** in **1% skimmed milk in WB Wash Buffer**
    a. Incubate the membrane in the primary antibody **overnight in +4°C**
8. Wash the membrane three times with WB Wash Buffer, 5 minutes on a shaker
9. Dilute **rabbit-anti-Mouse secondary antibody 1:10 000** in **1% skimmed milk in WB Wash Buffer**
    a. Incubate the membrane in the secondary antibody for **1h at room temperature**
10. Wash the membrane three times with WB Wash Buffer, 5 minutes on a shaker
11. Mix equal volumes of SuperSignal West Pico PLUS reagents, and incubate the membrane for **5 minutes at room temperature**
12. Visualize the membrane with x-ray film exposure.

WB Wash Buffer = non sterile TBS + 0,1% Tween20

Actin (Bethyl labs: A300-491A) Western blot
Antibody produced in Rabbit Salmikangas 2020

1. Pipette 5µg of each pretreated and denatured protein lysate and protein ladder on SDS-PAGE gel
2. Run the gel with **100V constant** for roughly **1,5 hours**, or until the leading buffer nears the end of the gel
3. Remove the gel from the holder and stack it in between the **Trans-Blot Turbo Transfer Pack.** The bottom and top portions are labeled, and the gel comes in between them.
4. Transfer the proteins to the PVDF membrane included in the transfer pack with Bio-Rad **Trans-Blot Turbo.** Use the pre-installed protocol **Mixed molecular weights**, 1,3A, 7min.
5. Block the membrane with **5% skimmed milk in WB Wash Buffer**
6. Wash the membrane three times with WB Wash Buffer (Optional), 5 minutes on a shaker
7. Dilute **Actin primary antibody 1:100 000** in **1% skimmed milk in WB Wash Buffer**
    a. Incubate the membrane in the primary antibody **overnight in +4°C**
8. Wash the membrane three times with WB Wash Buffer, 5 minutes on a shaker
9. Dilute **mouse-anti-Rabbit secondary antibody 1:10 000** in **1% skimmed milk in WB Wash Buffer**
    a. Incubate the membrane in the secondary antibody for **1h at room temperature**
10. Wash the membrane three times with WB Wash Buffer, 5 minutes on a shaker
11. Mix equal volumes of SuperSignal West Pico PLUS reagents, and incubate the membrane for **5 minutes at room temperature**
12. Visualize the membrane with x-ray film exposure.

WB Wash Buffer = non sterile TBS + 0,1% Tween20

CM2B4 (Santa Cruz, sc-136172) Western blot
Antibody produced in Rabbit Salmikangas 2019

1. Pipette 5µg of each pretreated and denatured protein lysate and protein ladder on SDS-PAGE gel
2. Run the gel with **100V constant** for roughly **1,5 hours**, or until the leading buffer nears the end of the gel
3. Remove the gel from the holder and stack it in between the **Trans-Blot Turbo Transfer Pack.** The bottom and top portions are labeled, and the gel comes in between them.
4. Transfer the proteins to the PVDF membrane included in the transfer pack with Bio-Rad **Trans-Blot Turbo.** Use the pre-installed protocol **Mixed molecular weights**, 1,3A, 7min.
5. Block the membrane with **5% skimmed milk in WB Wash Buffer**
6. Wash the membrane three times with WB Wash Buffer (Optional), 5 minutes on a shaker
7. Dilute **CM2B4 primary antibody 1:1000** in **1% skimmed milk in WB Wash Buffer**
    a. Incubate the membrane in the primary antibody **overnight in +4°C**
8. Wash the membrane three times with WB Wash Buffer, 5 minutes on a shaker
9. Dilute **mouse-anti-Rabbit secondary antibody 1:10 000** in **1% skimmed milk in WB Wash Buffer**
    a. Incubate the membrane in the secondary antibody for **1h at room temperature**
10. Wash the membrane three times with WB Wash Buffer, 5 minutes on a shaker
11. Mix equal volumes of SuperSignal West Pico PLUS reagents, and incubate the membrane for **5 minutes at room temperature**
12. Visualize the membrane with x-ray film exposure.

WB Wash Buffer = non sterile TBS + 0,1% Tween20

Appendix 4. qPCR protocols

Roche Universal ProbeLibrary qPCR

Reaction setup (1 qPCR reaction):

	ul
Forward Primer 10uM	0.5
Reverse Primer 10uM	0.5
UPL Probe# 10uM	0.2
UPL MasterMiX	5
DNA template	100ng
Water	ad 10µl

Thermal cycling protocol:

Step 1. Initial DNA denaturation/polymerase activation
- 95°C, 10min

Step 2. DNA denaturation
- 95°C, 10s

Step 3. Annealing
- 60°C, 30s

Step 4. Elongation
- 72°C, 1s
- Plate read/Acquisition

Repeat to Step 2 44 times (total 45 cycles)

Step 5. Melting curve
- 65-95°C
- 0,5°C increment

Step 6. Cooling
- 40°C, 30s

SsoAdvanced Universal SYBR Green Supermix

Reaction setup (1 qPCR reaction):

	ul
Forward Primer 10uM	0.5
Reverse Primer 10uM	0.5
SYBR GREEN MasterMiX	5
DNA template	100ng
Water	ad 10µl

Thermal cycling protocol:

Step 1. Initial DNA denaturation/polymerase activation
- 95°C, 30s

Step 2. DNA denaturation
- 95°C, 15s

Step 3. Annealing and elongation
- 60°C, 30s
- Plate read/Acquisition

Repeat to Step 2 44 times (total 45 cycles)

Step 4. Melting curve
- 65-95°C
- 0,5°C increment

Step 5. Cooling
- 40°C, 30s

Appendix 5. Example images of siRNA transfection optimization

MCC13 24-well plate, 1ul Lipofectamine 2000, 50nM siGLO, 1/100s exposure AUTO settings ISO 400

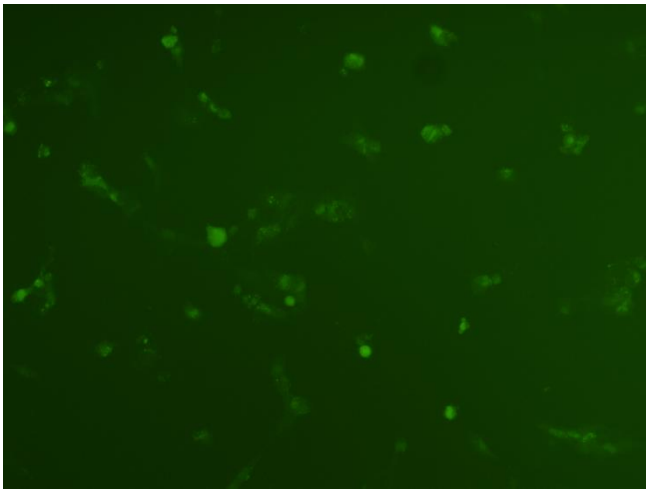

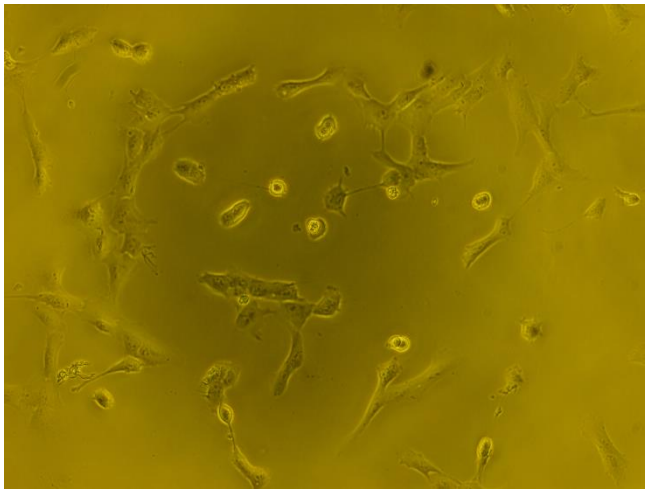

WaGa 24-well plate, 1ul Lipofectamine 2000, 50nM siGLO, 1/100s exposure AUTO settings ISO 400

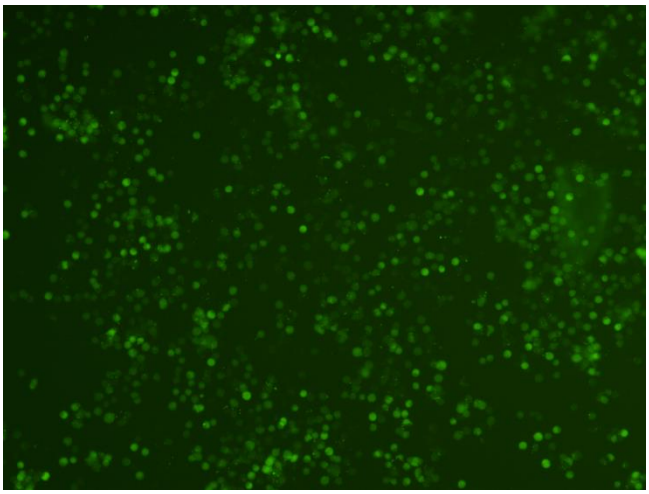

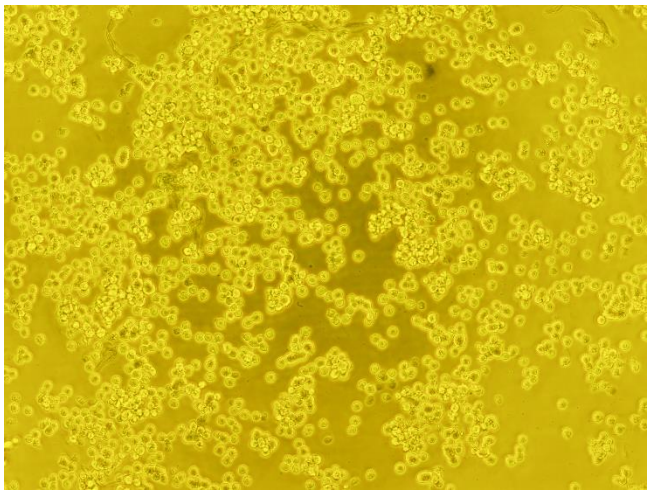

MCC13 24-well plate, 2ul Lipofectamine 2000, 50nM siGLO, 1/100s exposure AUTO settings ISO 400

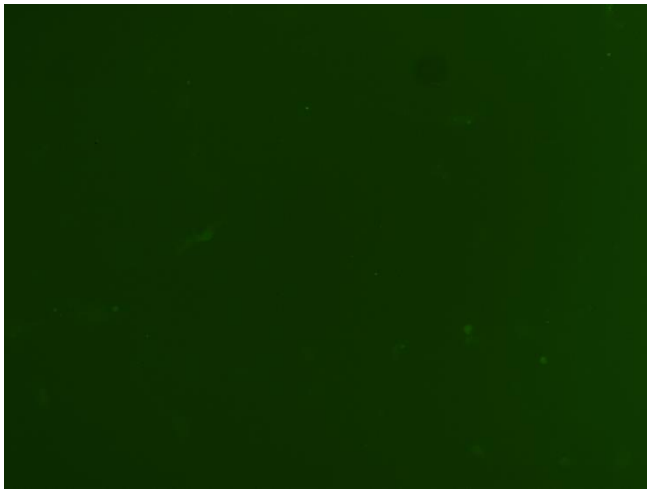

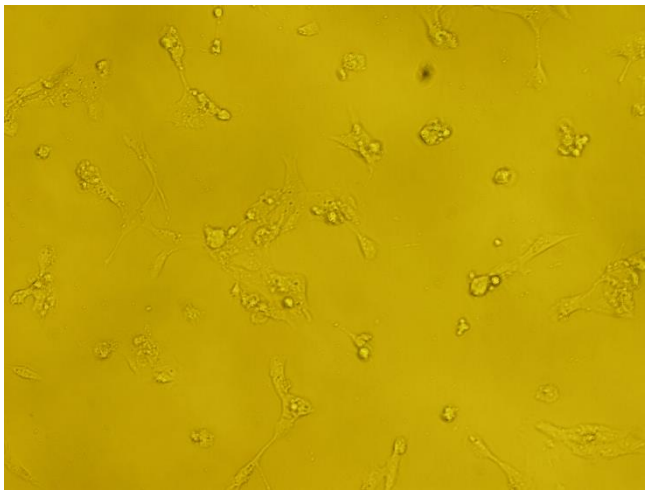

WaGa 24-well plate, 2ul Lipofectamine 2000, 50nM siGLO, 1/100s exposure AUTO settings ISO 400